Schweizerische Eidgenossenschaft
Confédération suisse
Confederazione Svizzera
Confederaziun svizra

Eidgenössisches Departement für
Umwelt, Verkehr, Energie und Kommunikation UVEK

Bundesamt für Energie BFE

Final report 18. April 2012

Erweiterung und Validierung der CRFD (Computational Reactive Fluid Dynamics)-Simulation für neue motorische Brennverfahren und Kraftstoffe

---

LAV
Laboratorium für Aerothermochemie und Verbrennungssysteme
Aerothermochemistry and Combustion Systems Laboratory

Competence Center
Energy and Mobility
5232 Villigen PSI
Switzerland

Tel. +41 (0)56 310 21 11
Fax +41 (0)56 310 27 17
ccem@psi.ch

Auftraggeber:
Bundesamt für Energie BFE
Forschungsprogramm Verbrennung
CH-3003 Bern
www.bfe.admin.ch

Kofinanzierung:
Swiss Competence Centre for Energy and Mobility (CCEM), CH-5232 Villigen/PSI
Forschungsvereinigung Verbrennungskraftmaschinen e.v. (FVV), D-60528 Frankfurt/Main
EU 7th Framework Programme, Project HERCULES-B

Auftragnehmer:
ETH Zürich
Institut für Energietechnik, Laboratorium für Aerothermochemie und Verbrennungssysteme
Prof. Dr. K. Boulouchos
ML J39
Sonneggstr. 3
CH-8092 Zürich
www.lav.ethz.ch

Autoren:
Yuri M. Wright, ETH Zürich, wright@lav.mavt.ethz.ch
Michele Bolla, ETH Zürich, bolla@lav.mavt.ethz.ch
Panagiotis Kyrtatos, ETH Zürich, kyrtatos@lav.mavt.ethz.ch
Peter Obrecht, ETH Zürich, obrecht@lav.mavt.ethz.ch
Stéphanie Schlatter, ETH Zürich, schlatter@lav.mavt.ethz.ch
Bruno Schneider, ETH Zürich, schneider@lav.mavt.ethz.ch
Konstantinos Boulouchos, ETH Zürich, boulouchos@lav.mavt.ethz.ch

BFE-Bereichsleiter: Sandra Hermle, sandra.hermle@bfe.admin.ch
BFE-Programmleiter: Stephan Renz, renz.btr@swissonline.ch
BFE-Vertrags- und Projektnummer: 153474 / 102688

Summary

The availability of predictive simulation tools has become indispensable in the optimization process of combustion devices. This project is directed towards the further improvement of a ‚high-fidelity' numerical model for fuel spray combustion, with particular emphasis on improvements of the quantitative predictions of heat release and emissions.

To this end, numerical and experimental approaches are combined: On the measurement side, a single-cylinder heavy-duty research engine has been commissioned and subsequently employed to establish a comprehensive dataset for engine model validation. An in-house high temperature high pressure optically accessible 'generic' combustion chamber has further been augmented with a hydrogen pre-combustion module, enabling data collection also at higher temperatures and for a broader range of fuels. Further data characterizing auto-ignition events of Diesel pilot sprays in lean premixed methane charges and subsequent flame propagation (dual fuel combustion) has been acquired by means of an in-house rapid compression/expansion machine with optical access.

The data-sets from these in-house experiments carried out during the course of this project are further supplemented by data from a large marine engine reference experiment installed at an industry partner (Wärtsilä Switzerland Ltd.) and additional data-sets documented in the literature. Based on this information, in-depth validation and further development of the Conditional Moment Closure (CMC) combustion model has been performed. The findings reported suggest that the model can capture a wide range of physical processes occurring in spray autoignition. As a consequence, the model is capable of providing excellent qualitative and to large extent very good quantitative predictions of ignition delays and locations, flame lift-off heights, heat release rates/pressure rise as well as NO_x emissions and soot volume fraction distributions.

The project is structured in five work packages (APs), some of which are subdivided in an experimental and numerical part. These are summarized briefly as follows:

AP1: A heavy-duty single cylinder engine test rig with well-defined intake and exhaust plenum conditions has been commissioned and subsequently employed to generate a comprehensive dataset for model validation. Variations include on the one hand changes in the air path, i.e. air temperature and pressure combinations, especially also towards low temperature conditions typical for Miller valve timings. Secondly, the influence of parameters relating to the fuel path have been systematically investigated, in particular the effect of injection pressure and injection strategies, which including piloted injections. The assembled matrix constitutes a highly challenging dataset for combustion and emission models. This data and the test rig will be used in two approved follow-up projects of the Swiss Innovation promotion agency (KTI) and the Competence Centre Energy and Mobility (CCEM) for further experimental investigations as well as model validation and development.

In work package **AP2a,** the influence of the fuel composition on the injection process, spray formation, ignition and combustion for seven fuels which consist of six Fischer-Tropsch fuels (with varying paraffinic, olefinic, naphthenic and aromatic contents) plus a reference Diesel synthetic has been characterised by means of experiments carried out in the optically accessible high pressure and temperature cell (HTDZ) of LAV. In order to reach the high gas temperatures required for short ignition delays comparable to those found in Diesel engines, the test rig has further been supplemented with a new Hydrogen pre-combustion module in this project. The project was co-funded by the successfully completed project „Future Fuels Diesel" of the Forschungs-Vereinigung Verbrennungskraftmaschinen (FVV).

AP2b and AP4b: Experiments with diesel spray pilot injection in a methane air mixture under various conditions have been performed on an optically accessible single stroke machine installed at ETH. Optical and transient data of the dual fuel combustion processes were acquired for different operating conditions. The successful application of the developed combustion model for dual fuel combustion could be shown. Excellent agreement of computed and experimentally obtained ignition delay times as well as ignition locations and initial flame shapes with respect to the amount of methane in the ambient gas mixture is observed. Co-funding for both work packages is provided by two projects of the Ger-

man FVV namely “Piloteinspritzung” and “Miller/Atkinson”, the former of which has been successfully completed.

AP3: This package consists of model validation by means of the broad range of experimental data from an the-house heavy-duty engine, the single stroke rapid compression/expansion machine and four different optically accessible spray test rigs of different sizes. In addition to the successful validation of heat release rate predictions, ignition timing and location, flame lift-off heights for the generic test rigs, sensitivity analyses have been reported to various sub-models and uncertainties in the boundary conditions stemming from the experiment. Furthermore, on the emission side, qualitative trends of NO_x emission have been demonstrated for the heavy-duty engine for a range of operating conditions and the influence of EGR is well reproduced. In addition the model has successfully been extended by a two-equation soot model implemented in the CMC context. Excellent predictions of soot volume fraction distributions are reported for a broad range of oxygen contents at two different engine relevant pressures.

AP4a: As part of AP4a, measurements from a medium speed diesel engine (Wärtsilä 6L20) have been used to study ignition delay as a function of in-cylinder conditions during injection. Particular emphasis is placed on conditions with different Miller valve timings and two-stage turbo-charging configurations, resulting in very broad temperature and pressure ranges. A correlation for ignition delays for this broad range of operating conditions has been successfully developed, based on a three-Arrhenius model which was developed in the framework of the FVV project “Kraftstoffkennzahlen” using shock tube data and co-funded by the Swiss Office of Energy (BfE). The engine is part of the CCEM-LERF engine test-bed, located in PSI, Villigen, and is further co-funded by the CCEM - CELaDE and EU FP7 HERCULES-B projects.

AP5: Publication and reporting has been carried out in parallel to the work packages and resulted in several peer reviewed journal publications and a number of conference proceedings. In addition, annual and intermediate reports have been provided to the Swiss Office of Energy (BfE).

Table of Contents

1 Introduction

Diesel engines are among the most efficient energy converters available today and hence widely employed for power generation and surface transport; for the latter in particular in heavy-duty scenarios characterized by a substantial share of running vs. investment costs.

Diesel engine out emissions contain large amounts of particulate matter and NO_x, which exhibit a trade-off behaviour. Due to the overall lean operation of compression-ignition engines, three-way catalyst concepts as in use for spark ignited premixed engines operated at stoichiometric conditions cannot be employed. A wide range of concepts are hence currently investigated by researchers and industry world-wide to find solutions to address the overall environmental impact, i.e. to maintain good efficiency (low CO_2) and at the same time reduce NO_x and soot. While substantial progress has been made on the after-treatment side also for Diesel engines, e.g. by employing particulate filters and Selective Catalytic Reduction techniques, substantial improvements are still achievable by in-cylinder measures.

In this project, experimental and numerical techniques are hence combined in an effort towards improving the understanding with respect to in-cylinder combustion processes and to further develop and validate numerical tools toward improved predictions of combustion and emission formation.

The report is structured by work packages, for which a brief introduction and conclusions are presented at the beginning/end of the respective chapters.

2 Work package AP1

As part of AP1, measurements were conducted on a medium duty, single-cylinder research engine setup in ETH Zurich. The focus of the measurements was to create a comprehensive data-set for the purpose of 3D Computational Reactive Fluid Dynamics (CRFD) simulation validation. More specifically of interest was the study of mixture formation during the ignition delay time, which leads to effects which can be observed during premixed and diffusion combustion, as well as affecting NO_x emissions. To this extent, inlet conditions, main injection duration and timing, as well as pre-injection timing were varied, in order to study the chemical and physical sensitivities of the apparent combustion processes.

2.1 Experimental Setup

The single cylinder research diesel engine used is based on a MTU 396 heavy duty engine. The engine cylinder has a displacement volume of 3.96 liters, with a 165 mm bore and a 185 mm stroke. Pressurized air is supplied to the inlet via a centralized air supply system. The system has a steam heater to heat up incoming air, and a water cooler is placed before the engine to allow precise inlet air temperature control. Exhaust gas pressure can be regulated via an exhaust throttle. The engine is fitted with a common rail injection system, which allows a maximum of 3 injections per cycle. The injection system allows injection pressures up to 1400 bar and it is controlled through a freely programmable engine control unit (ECU) supplied from Bodensee Steuergeräte (BSG).

2.2 Measurement Matrix

The measurement series involved the variation of inlet parameters, in order to evaluate their effects on ignition delay, premixed and diffusion combustion and NO_x emissions. The injection duration was also varied between 1 ms, 1.5 ms and 2 ms, corresponding to ~4 bar, ~8 bar and ~12 bar Brake Mean Effective Pressure (BMEP), to vary the load of the engine, as well as the amount of diffusion combustion at constant inlet conditions.

Apart from single injections, investigations with pre-injections were carried out to assess their effect on main injection ignition delay and NO_x formation. Throughout all measurements the engine speed was held constant at 1000 RPM, as was the Start of Injection (SOI) of the main injection at -5 degrees CA and the injection pressure at 1000 bar.

2.2.1 Single Injection

For the investigations with single injections, the inlet temperature and pressure were varied in order to achieve different conditions at Top Dead Center (TDC). The chosen inlet pressures were 1.3, 1.4, 1.5, 1.6, 1.7 and 2.6 bar. These translate to pressures at TDC of 40, 44, 47, 50, 53 and 80 bar. Correspondingly, inlet temperatures were varied between 17 °C, 42 °C and 67 °C, which translate to ~810 K, ~860 K and ~910 K at TDC. These temperatures were chosen to achieve constant density when combining different inlet pressures and temperatures. This allows the de-coupling of temperature effects to the chemistry, from physical spray effects (barring the effects of increased evaporation at higher temperatures, which should not be very significant at very high temperatures). In total the measurement matrix contains 76 points of varying temperature, pressure and injection duration.

2.2.2 Pre-Injection

In the investigations with pre-injections the total injected mass was held constant to correspond to the injected mass from the single injection investigations (1ms, 1.5ms and 2ms). The inlet temperature was held constant at 17° C (~810 K at TDC), in order to study the pre-injection effects with the longest possible ignition delay. Inlet pressure was again varied between 1.3, 1.4, 1.7 and 2.6 bar. The pre-injection duration was kept constant at 0.5 ms, which was the shortest repetitive injection duration possible with the injector used. The gap between pre- and main injection was varied between 1 and 1.3 ms. Finally, the SOI of the main injection was varied between -5 degrees crank angle (CA) to enable comparisons with the single pulsed cases as well as -3 and -1 degrees CA, in order to achieve the

same indicated efficiency with the single injection cases with the same inlet and fuel mass conditions. Overall, the measurement matrix with pre-injections contains 35 points.

2.3 Injector Rate Measurements

In order to have reliable measurement results, to be used for simulation validation, the repeatability of the injection, especially in the cases of multiple injections is paramount. The injection system used in this investigation was designed to have very small cycle-to-cycle variations for short, consecutive injection signals. To check the repeatability of the injection system, the injection rate was measured for consecutive cycles using an injection rate analyzer specifically designed for heavy duty injection systems. The injection rate measured was also used in order to provide an input to the simulation, and allow the accurate modeling of the injection process. Sample injection rate measurements for 1000 bar and 1ms single injection duration, 2 ms single injection duration and 0.5 ms pre-injection with 1.5 ms main injection and a 1 ms gap are shown in Figure 1 to Figure 3 below. The plots contain the injection rate trace, followed by the injection rail pressure trace.

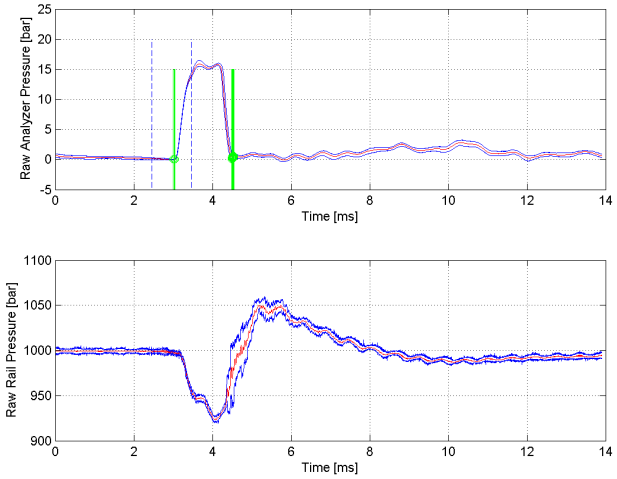

Figure 1: Injection rate and rail pressure trace for 1000 bar, 1 ms injection signal. The green vertical lines denote the start and end of the single injection pulse. The red lines show the average injection rate and pressure. The blue lines show the most extreme cycles recorded.

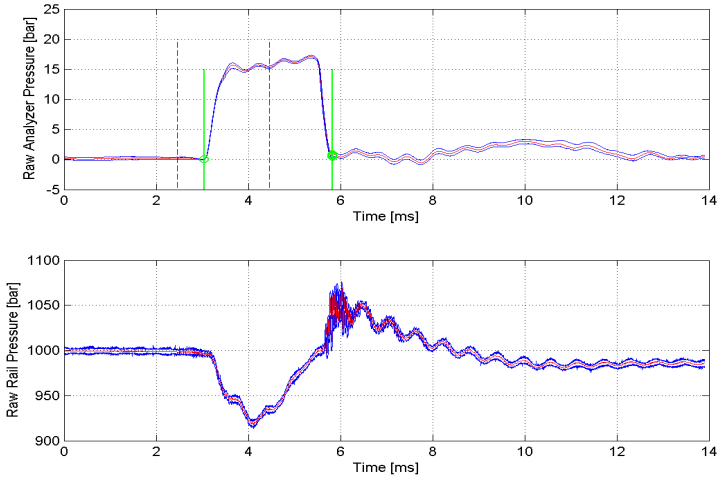

Figure 2: Injection rate and rail pressure trace for 1000 bar, 2 ms injection signal. The green vertical lines denote the start and end of the single injection pulse. The red lines show the average injection rate and pressure. The blue lines show the most extreme cycles recorded.

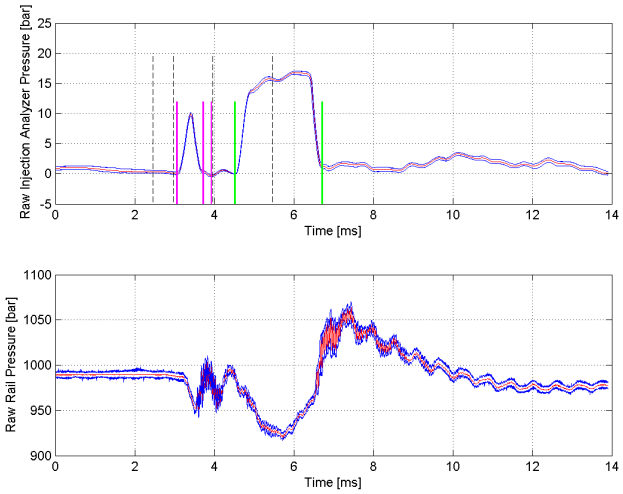

Figure 3: Injection rate and rail pressure trace for 1000 bar, 0.5 ms pre-injection, 1 ms gap and 1.5 ms main injection signal. The magenta and green vertical lines denote start and end of the pilot and main injection pulses, respectively. The red lines show the average injection rate and pressure. The blue lines show the most extreme cycles recorded.

Overall, the injector measurements showed very good repeatability of the injection rate and mass, even with very short injection durations and with consecutive short injections. The overall performance of the injection system was deemed adequate for the investigations to be undertaken for pre-injection signals down to 0.5 ms.

2.4 Engine measurement Results

The results relevant for simulation validation obtained in this campaign are mainly measured pressure traces and NO_x emissions, as well as calculated Heat Release Rate (HRR). The calculation of the HRR was performed using the thermodynamic calculation software WEG [1], which has been developed in-house. With the use of two-zone modeling and various sub-models for the calculation of heat losses and blow-by, WEG allows the calculation of HRR taking into account the influences of such losses. Additionally, coupled with the input of the measured injection rates, WEG has the ability to output information about in-cylinder air-fuel mixing such as apparent mixing rates. Sample pressure and apparent HRR curves for 2ms injection duration, 2.6 bar inlet pressure and 17° C inlet temperature are shown in Figure 4 below:

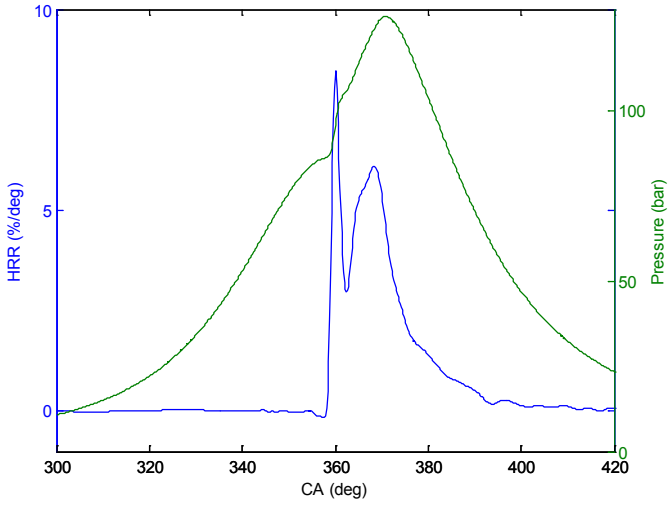

Figure 4: Measured pressure and HRR for inlet pressure 2.6 bar, inlet temperature 17° C and 2 ms injection duration.

2.4.1 Single Injection

A major advantage an experimental setup such as the current one has is that the independent setting of inlet temperature, pressure and injection duration can be used to study the effects of premixed vs. diffusion combustion, as well as effects of temperature on NO_x emissions. By setting different injection durations at the same inlet conditions, one can try to study in which part of combustion the NO_x formation takes place. Figure 5 below shows the HRR for constant inlet conditions but varying injection durations. On the other hand, the effects of different temperatures or pressures on ignition delay and HRR can be investigated.

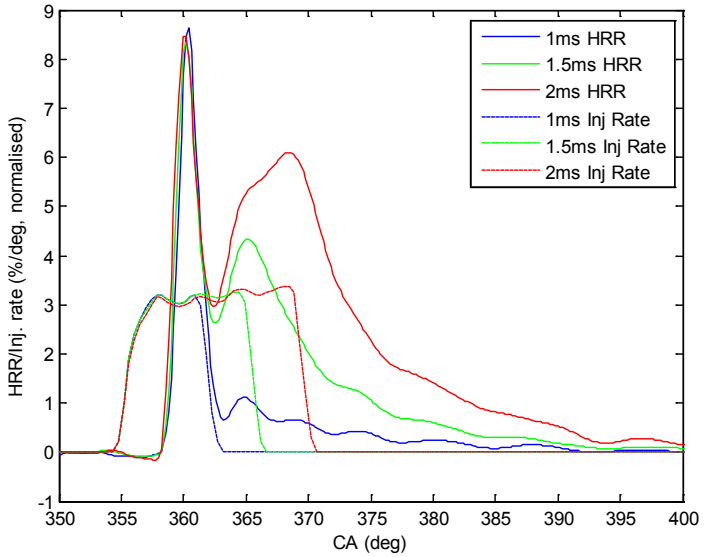

Figure 5: HRR for 1 ms, 1.5 ms and 2 ms injection durations at 2.6 bar and 17° C inlet pressure and temperature.

Figure 6 and Figure 7 below show the HRR at varying inlet temperature and constant inlet pressure and injection duration.

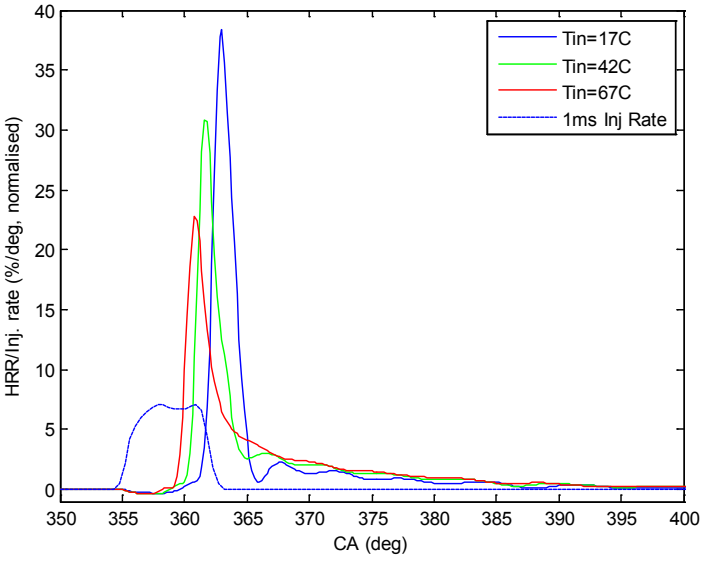

Figure 6: HRR for 1 ms injection duration and 1.3 bar inlet pressure at varying temperature.

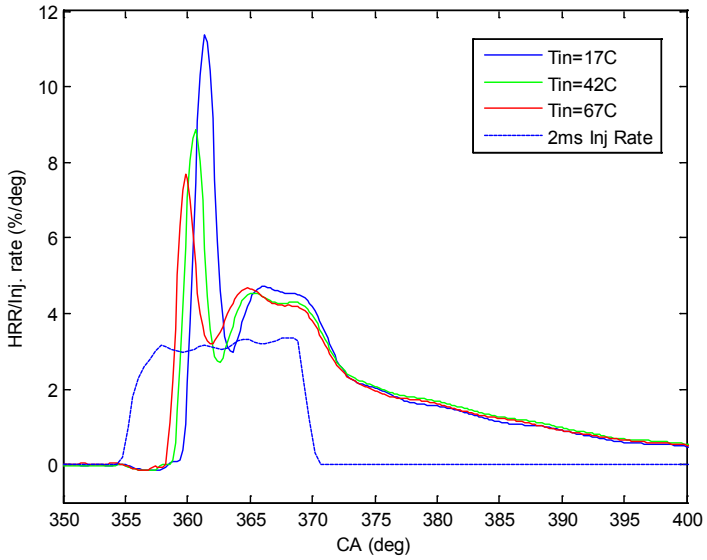

Figure 7: HRR for 2 ms injection duration and 1.3 bar inlet pressure at varying temperature.

These investigations allow the establishment of trends for HRR and NO_x formation, which can be used to validate combustion and emissions models used in CRFD. Sample NO_x measurements for constant inlet pressure and varying inlet temperature and injection duration can be seen in the figures below:

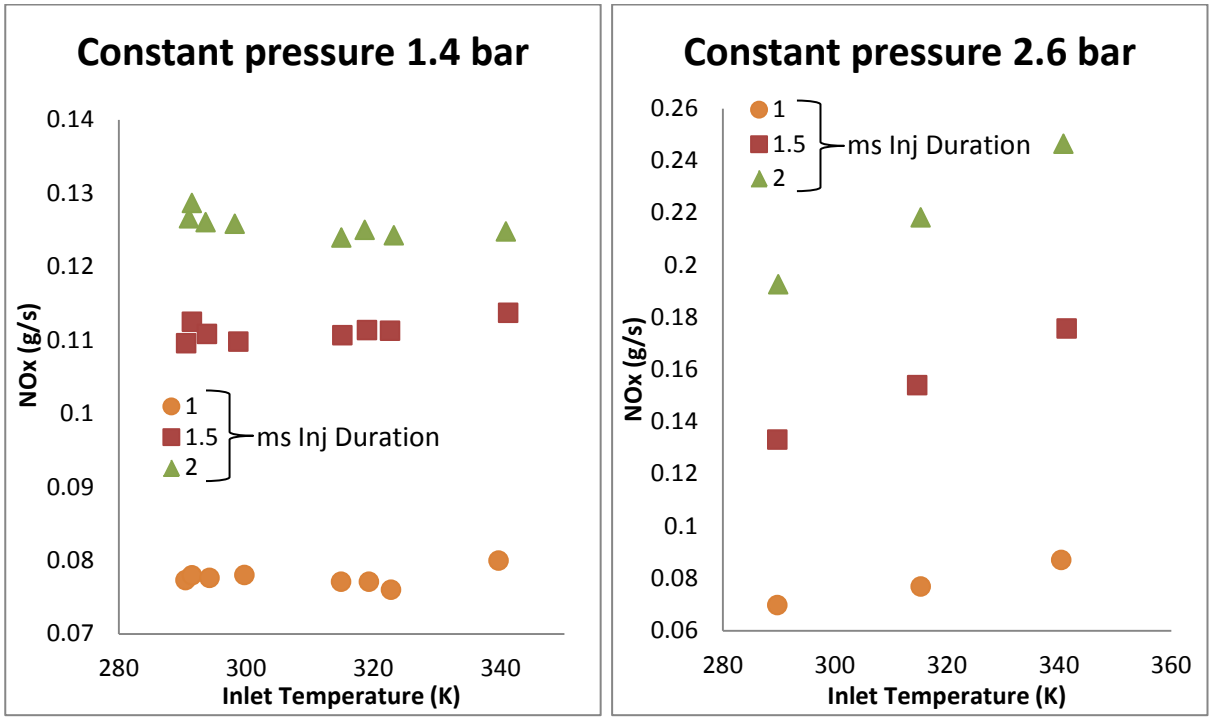

Figure 8: NOx for constant inlet pressures of 1.4 and 2.6 bar for varying temperature and injection duration.

The NO_x emission measurements shown show the changing of trend of NO_x emission with temperature, depending on inlet pressure and injection duration. The results show a very high increase in NO_x emissions with temperature at high inlet pressures, contrary to low pressures where there is very little change in the emissions caused by the inlet temperature change.

The NO_x emissions are plotted as grams/second (g/s) instead of the more conventional unit g/kWh, since the power output of this engine is heavily influenced by the charge air pressure i.e. for constant injection duration, a higher inlet pressure will result to more positive work done in the gas exchange cycle, artificially increasing the power output of the engine.

2.4.2 Pre-Injection

The introduction of a pre-injection before the main injection allows the study of its effects on ignition delay, HRR and NO_x emissions. Figure 9 to Figure 11 below illustrate the effect of pre-injection on HRR at varying conditions.

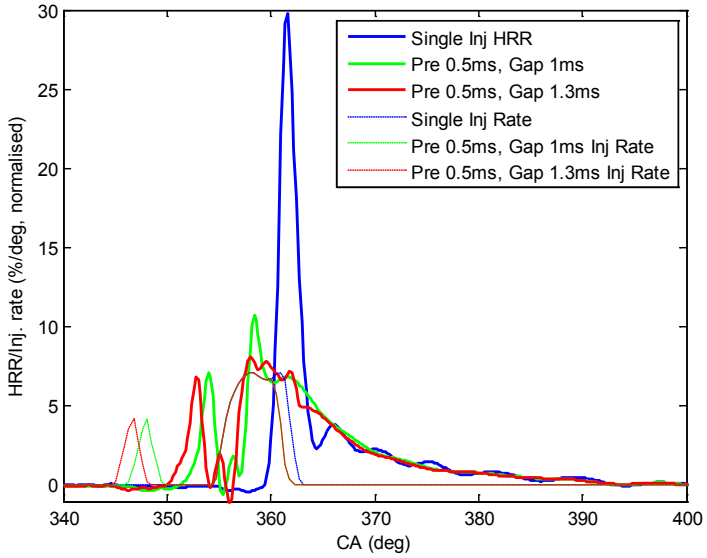

Figure 9: HRR for 1 ms injection duration, 2.6 bar and 17° C inlet pressure and temperature, with and without pre-injection.

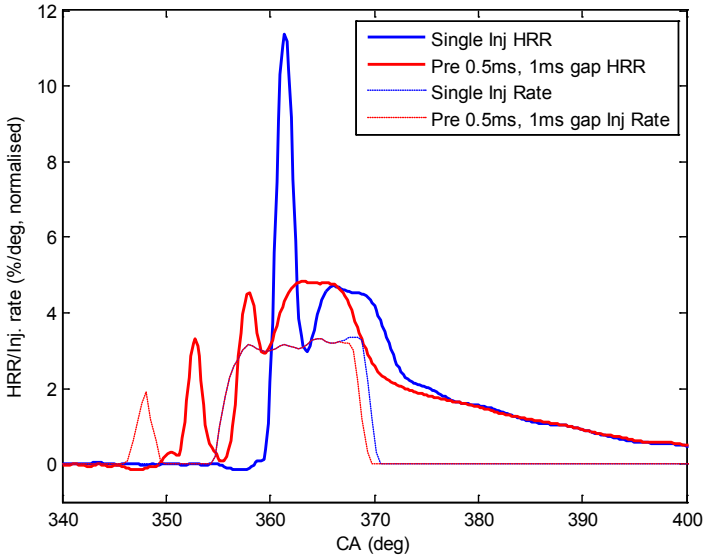

Figure 10: HRR for 2 ms injection duration, 1.3 bar and 17° C inlet pressure and temperature, with and without pre-injection. Identical timings for main pulse for both injection cases.

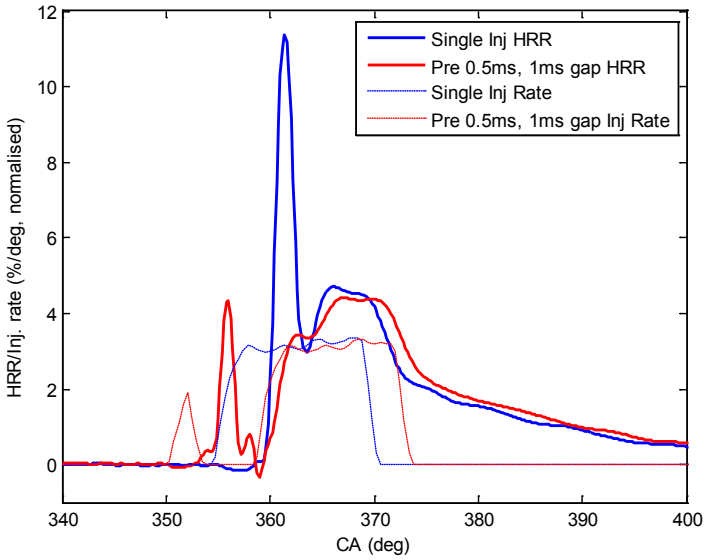

Figure 11: HRR for 2 ms injection duration, 1.3 bar and 17° C inlet pressure and temperature, with and without pre-injection. The main pulse of the single injection case is shifted to obtain identical main ignition timing.

The figures above show a significant decrease of main injection ignition delay at these conditions, when using a pre-injection. The reduction in ignition delay leads to a decrease of premixed combustion and pressure rise rate, effectively reducing emissions and potentially increasing the longevity of the engine. in all pre-injection cases the total fuel injected was kept equal to the relevant case with single injection.

In Figure 9 the effect of different dwell times between pre and main injection is shown. Small differences in dwell time have been shown to significantly affect gaseous emissions. This is a very interesting topic for future investigations using CRFD.

Figure 10 and Figure 11 show the effects of different injection timings on HRR. In Figure 10 the main injection timing was kept identical to the single injection case. In Figure 11 the SOI was delayed to achieve the same cycle efficiency, in order to allow emission comparisons at constant specific fuel consumption.

Finally, the figures below show the effect of the introduction of pre-injections to NO_x emissions at varying inlet pressure and different injection durations, with constant main injection SOI.

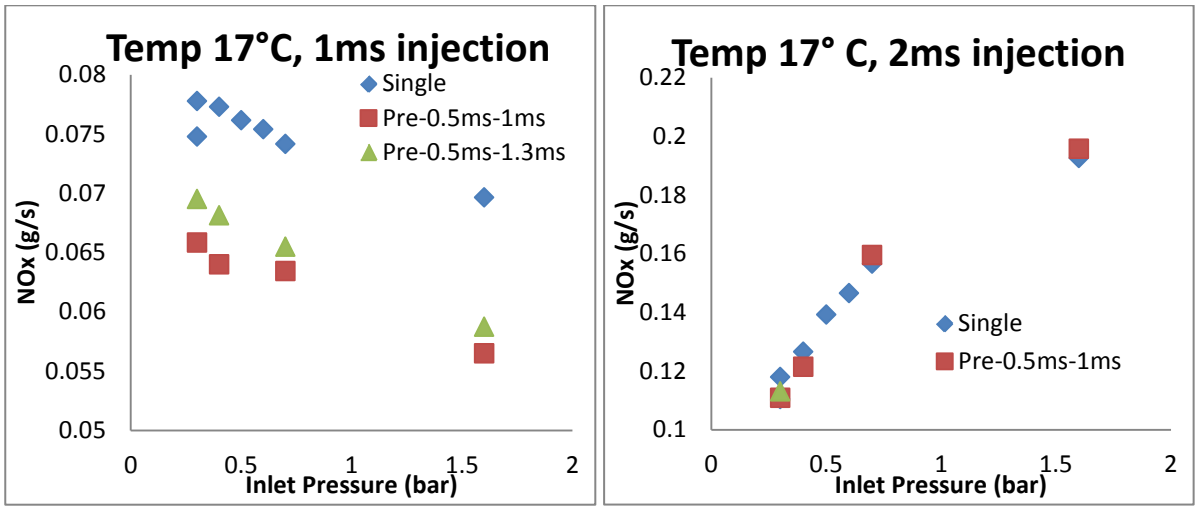

Figure 12: HRR for 1 ms injection duration, 2.6 bar and 17° C inlet pressure and temperature, with and without pre-injection.

2.5 Conclusions

In all, the measurements obtained so far from the single-cylinder test-bench have shown interesting trends in terms of combustion and NO_x formation at different inlet pressure and temperature conditions. The accurate measurement and calculation of various engine and injection parameters are hoped to aid in the development and calibration of CRFD models which will aim to capture observed trends and assist in future engine development.

Future measurement campaigns will aim to expand on current observations, and provide further understanding for NO_x and soot formation under various in-cylinder conditions. In order to simplify the simulation of chemical reactions needed for complex, multi-component diesel fuels, it is planned to fit a newly designed fuel system which will be able to handle heptane and heptane/toluene surrogates. This is expected to considerably increase the understanding of processes in-cylinder, since direct modeling of chemical processes is possible with single component fuels.

2.6 Major achievements

- Development of a high-fidelity test-bench, to be used for investigations into combustion and emission formation, and provision of validation data for diesel engine CRFD model development
- First investigations of the effects of inlet charge conditions on combustion and NO_x formation, with specific focus on high ignition delay conditions.
- Provision of a solid basis for further investigations into combustion and emission formation at varying charge air conditions

The test-bench will be used in the future within a KTI-funded project, to conduct research on the effects of Miller valve timing, Exhaust Gas Recirculation (EGR) and multiple injections on combustion and emission formation (KTI No. 13859.1, approved, start date 1st June 2012), with *ABB Turbosystems AG* as an industrial partner. This project is part of a larger CCEM-funded project, on “In-cylinder emission reduction in large diesel engines” (accepted), along with academic partner *Paul Scherrer Institut*, and additional industrial partners *Wartsila Finland OY* and *DUAP AG*. Within the CCEM project, the test-bench measurement results are aimed to provide support for CRFD simulation model development and background for the development of a high-pressure EGR system for large diesel engines.

3 Work package AP2a

3.1 Introduction

Work package AP2a investigates the influence of the fuel composition on the injection process, spray formation, ignition and combustion. The fuels considered are summarized in Table 7 (see Appendix) consist of seven synthetic Fischer-Tropsch fuels with varying paraffinic, olefinic, naphthenic and aromatic contents plus a reference Diesel.

The experiments were carried out in the high pressure and temperature cell (HTDZ) of the LAV. In order to reach the high gas temperatures required for short ignition delays comparable to those found in Diesel engines the HTDZ was supplemented with a new Hydrogen pre-combustion module for this project.

3.2 Experimental Setup

Figure 13 shows the measurement setup used for the experiments in this work package. The HTDZ permits very good optical access for the observation of the spray propagation, ignition and combustion: The Mie light scattering technique is used for the measurement of the fuel spray propagation

(liquid phase, illumination through the side windows), the ultraviolet chemiluminescence of the OH radical is used for the observation of ignition and combustion.

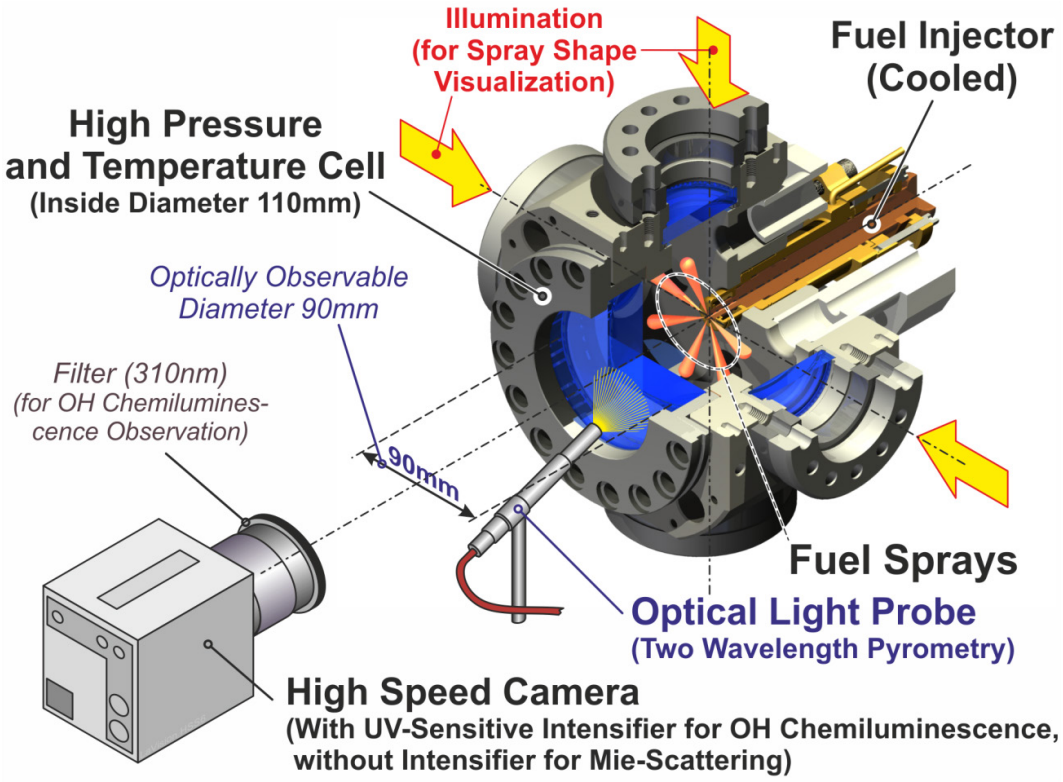

Figure 13: Setup of the high pressure cell (HTDZ) for the experiments in this work package.

Time resolved images of the scattered light resp. the OH-Chemiluminescence are recorded with a high speed camera looking through the large window of the cell onto the seven fuel sprays of the Common Rail injector (Bosch magnetic type CRI 2.2). Additionally an optical light probe collects light emitted by the glowing soot for analysis with the two/three wavelength pyrometry method to calculate the global soot temperature and the KL value (representative of the soot concentration). The heat release of the combustion is calculated from the cell pressure trace with software specially adapted to the conditions found in the constant volume HTDZ. The ignition delay can be determined either from the calculated heat release rate or from the OH-Chemiluminescence images.

3.3 Parameters

To isolate the influence of the fuel composition on the spray propagation (liquid phase penetration and spray volume) the spray propagation was measured at two gas temperature levels with identical gas densities (19.4 kg/m^3) in a Nitrogen atmosphere: One temperature (T_{Gas}=400 K, p_{Gas}=23 bar) was selected below, the other (T_{Gas}=650 K, p_{Gas}=38 bar) above the boiling curves of the investigated fuels. The experiments with ignition and combustion took place at a gas temperature of 950 K (p_{Gas}=55 bar, 19.4 kg/m^3) in air. The hydrogen pre-combustion in the cell reduced the oxygen level before the Diesel injection by 25 percent (corresponding to an oxygen based EGR rate of 25 percent). The standard measurement set included three injection pressures (rail pressures of 500 bar, 1000 bar and 1500 bar) and two (electric) injection durations (0.5 ms and 1.0 ms). The hydraulic injection delay and the amount of injected fuel are known from the earlier experiments on the injection equipment test bench of the LAV [2].

3.4 Results – Fuel Spray Propagation

Within the observable length of the fuel sprays the fuel type has no discernible influence on the axial spray propagation, even in measurements under evaporating conditions (T_{Gas}=650 K).

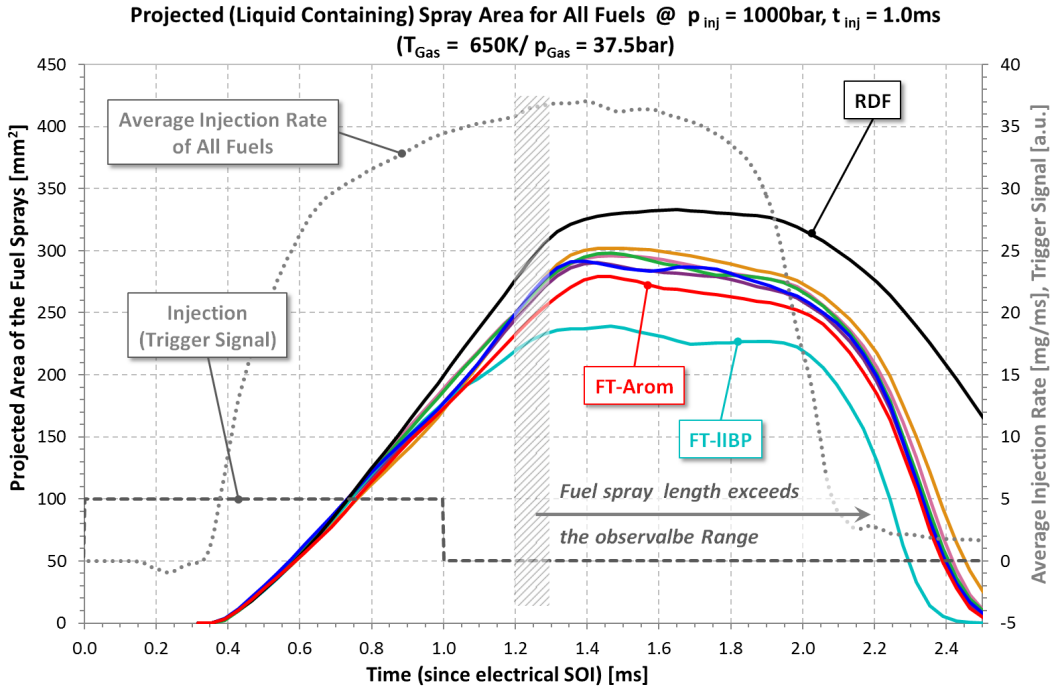

Figure 14: Projected spray area as a measure of the liquid containing spray volume under evaporating conditions (T_{Gas}=650 K). Injection pressure 1000 bar, injection duration 1.0 ms.

However, if we look at the (liquid containing) spray volume by means of the projected spray area in the images then the influence of the fuel boiling curves is clearly observable: Figure 14 shows the temporal evolution of the projected spray area under evaporating conditions for all fuels. About 1.2 ms after start of injection (SOI) the spray tip leaves the observable range, from then on until the end of injection (EOI) the area differences are only due to the different spray cone angles / spray widths. The fuel with the lowest boiling range (FT-IIBP: 134 °C to 307 °C) covers only about 70 percent of the spray area (approx. 60 percent of the volume) compared to the fuel with the highest boiling range (reference Diesel RDF: 163 °C to 355 °C).

3.5 Results – Ignition and Combustion

OH-Chemiluminescence images from a spray combustion event in the HTDZ are shown in Figure 15: 550 µs after hydraulic SOI the first four sprays have ignited, shortly afterwards the other sprays are burning as well. The reaction zones grow outwards along the spray axis, but not backwards towards the nozzle tip until after the end of injection (~1800 µs after SOI). The last image shows how the remaining fuel burns along the cell wall (at the limit and outside of the visible area). The combustion activity around the injector tip that can be seen in the last image originates from (undesired) post injections due to needle bouncing.

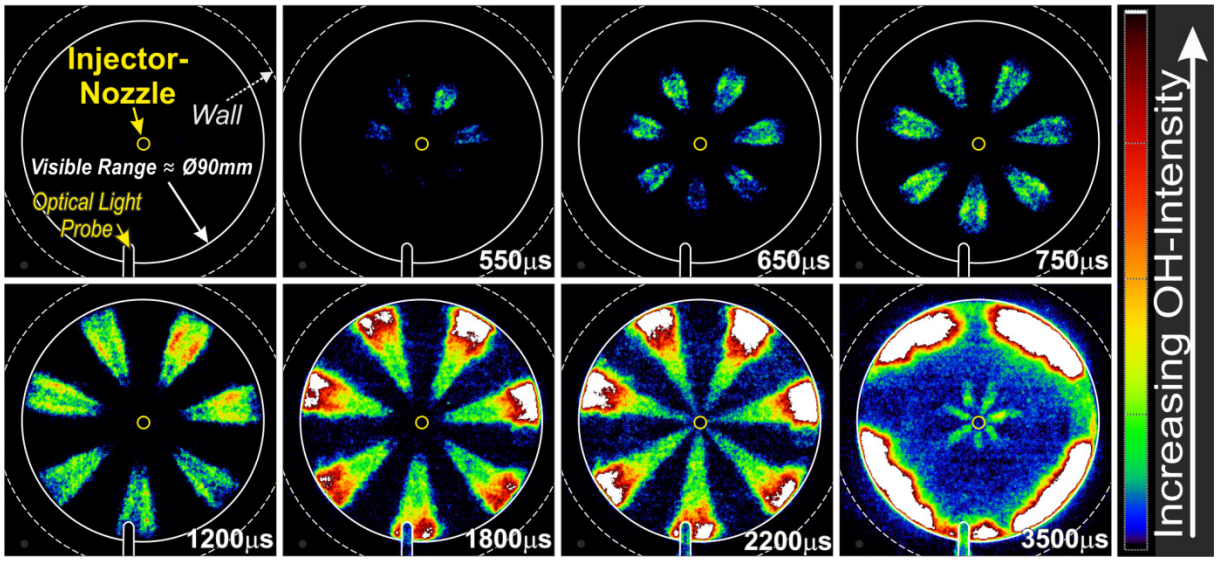

Figure 15: Temporal evolution of the combustion activity (OH-Chemiluminescence images, fuel FT-Base, p_{inj}=1000 bar, t_{inj}=1.0 ms, T_{Gas}=950 K, p_{Gas}=55 bar in air (25% EGR), times are with respect to the hydraulic SOI).

3.5.1 Ignition Delay

The cetane number describes the ignition quality of Diesel fuels; higher cetane numbers fuels have a shorter ignition delay. As can be seen in Figure 16 this is also the case in the measurements of the fuels investigated in this work package – but only as a general trend! For some fuels, for example FT-IIBP with a cetane number of 62.4 the ignition delays in the experiments in the HTDZ are longer than those of the fuel with the lowest cetane number (reference Diesel, cetane number 53). What can be seen as well in Figure 16 is that the variation of the ignition delay due to the variation of the fuel injection pressure *(→ changes the physical part of the ignition delay)* is higher than the variation due to the fuels cetane number *(→ changes the chemical part of the ignition delay)*.

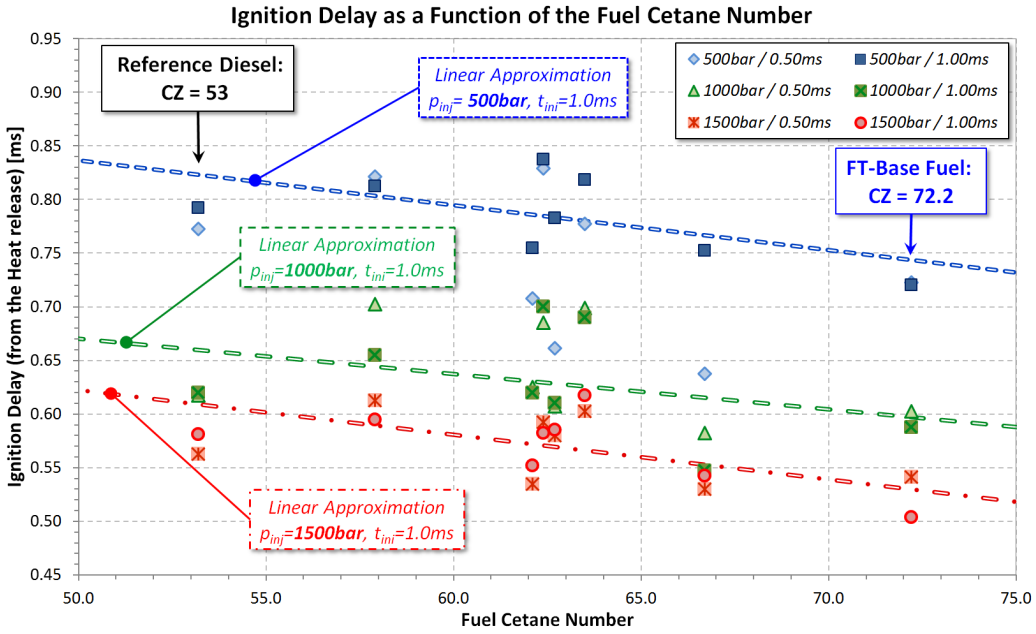

Figure 16: Ignition delay (derived from the heat release rate calculations) versus cetane number for all fuels and injection parameters. The linear approximations are calculated from the data with 1.0 ms injection duration only.

3.5.2 Heat Release Rate and Soot KL-Values (Soot Concentration)

Figure 17 shows the heat release rates and the soot KL-values for all fuels. The heat release rates exhibit the typical two phased Diesel combustion (premixed and diffusion combustion parts). The amount of the premixed phase differs between the fuels – a low boiling range and/or long ignition delay favors higher amounts of the premixed phase. The production of soot starts with the onset of the diffusion combustion phase, the maximum soot KL value (concentration) is reached after the maximum heat release rate. Towards the end of the combustion the soot oxidation process dominates and the soot concentration drops towards a common end value for all fuels.

This occurs in the HTDZ because the gas temperature after combustion remains at high levels for a long time (there is no expansion stroke as in engines), therefore the soot oxidation process has more time to oxidize (burn) most of the soot. In engines, the expansion stroke will reduce the gas temperature after combustion quickly, thereby stopping the soot oxidation process prematurely and "freezing" the soot particle concentration.

To compare exhaust gas soot concentration measurements of engines with the KL-value traces measured in the HTDZ it makes sense not to look at the end values but at values at some time after the combustion: For example 5 milliseconds after SOI the comparatively slow oxidation process of the naphthenic fuel (FT-Naph) results in a KL-value that is in the same order like the values for the reference Diesel and the aromatic fuel FT-Arom (the two fuels with the highest maximum KL-values). This could explain the results of engine test of the FVV project partner (IVK / University of Stuttgart) where the measured soot concentration in the exhaust gas has been much higher than expected for the naphthenic fuel composition [2].

Figure 18 shows the heat release rates and the soot KL-values for all fuels as in Figure 17 but with a shorter injection duration of 0.5ms.

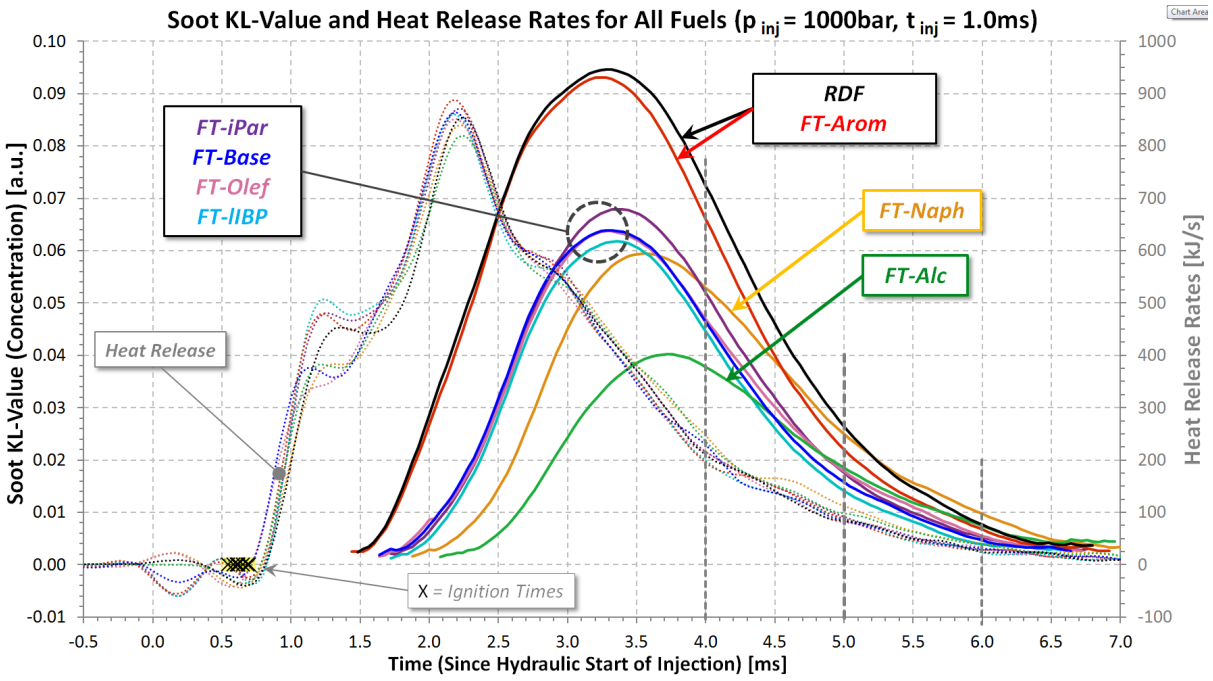

Figure 17: Heat release rates (dotted lines) and soot KL-values (soot concentration) for all fuels. T_{Gas}=950 K, p_{Gas}=55 bar, air (25% EGR), injection pressure 1000 bar, injection duration 1.0 ms.

The maximum heat release rate in Figure 18 is comparable to the heat release rate *of the premixed phase* in Figure 17, but the fuel required for the following intense diffusion combustion phase in Figure 17 is missing because of the shorter injection duration in Figure 18. Again the fuels with aromatic content have the highest KL-values; the fuel with alcoholic content has the lowest KL-values. The

slower soot oxidation process of the naphthenic fuel (FT-Naph) is also present in the experiments with the shorter injection duration.

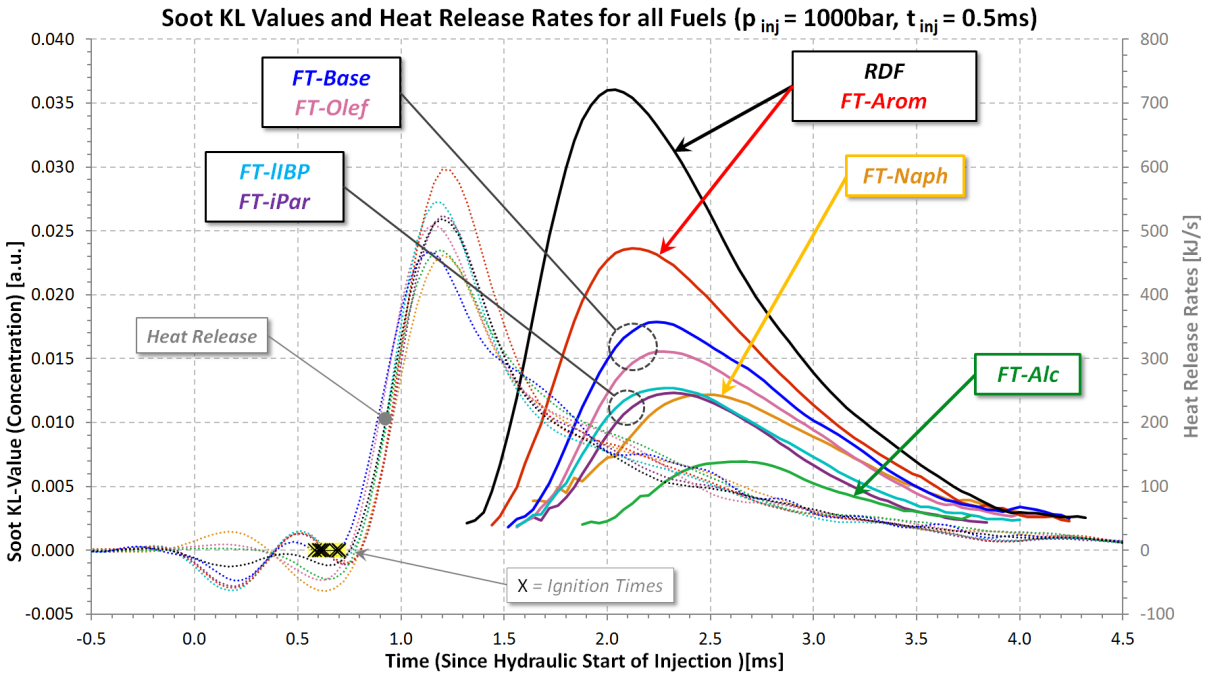

Figure 18: Heat release rates (dotted lines) and soot KL-values (soot concentration) for all fuels. T_{Gas}=950 K, p_{Gas}=55 bar, air (25% EGR), injection pressure 1000 bar, injection duration 0.5 ms.

These findings have been documented in [2].

3.6 Conclusions

The experiments in this project show that the varying composition of the investigated fuels have a considerable influence on the fuel ignition and combustion processes - fuel injection and fuel spray propagation however is very little affected by the fuel blend. The order of the ignition delays of the fuels follows approximately (but not absolutely consistently) their respective fuel cetane numbers, but on the other side the fuel injection pressure has a larger influence on the ignition delay than the fuel cetane number. During combustion the fuels with aromatic content show the highest maximum soot concentrations and the alcoholic blend shows the lowest soot concentrations as expected (measured by the KL value / soot pyrometry). Remarkable is the comparatively slow soot oxidation process towards the end of combustion of the naphthenic fuel blend – an indication why this fuel exhibited much higher than expected exhaust gas soot concentration levels in accompanying engine experiments.

The fuels investigated in this project have been selected because they are possible candidates for large scale synthetic Diesel fuel production using the Fischer Tropsch process. Future Experiments will complement these efforts by focusing especially on fuel surrogates (e.g heptane/toluene mixtures) on the one hand as well as oxygenated fuels and biofuel/Diesel blends. Experimental information hereto is instrumental with respect CRFD model development which aims at taking a step away from single component fuels such as heptane towards ‘real-life’ fuels. The latter constitutes a prerequisite for the development of accurate models of soot production/oxidation processes for further CRFD code development.

3.7 Major achievements

The influence of the composition of seven synthetic fuel blends and a reference Diesel on the complete chain of processes from fuel injection, spray propagation and evaporation to ignition and combustion including soot production/oxidation has been investigated and clarified. In combination with the

accompanying engine experiments (IVK/Univ. Stuttgart) it was possible to rate the synthetic fuels blends in respect to their suitability as a possible replacement for “normal” Diesel fuel produced from crude oil. These findings have been successfully presented at the FVV autumn conference in Fulda in 2011 and the final report can be found in [2].

3.8 Collaborations

AP2a is linked to the Project Nr. 940 „Future Fuels Diesel“ of the German Forschungs-Vereinigung für Verbrennungskraftmaschinen FVV (Project partner: IVK / University Stuttgart).

4 Work packages AP2b and AP4b

Piloted ignition finds its application in large bore stationary and ship engines. The main objective of these work packages is to assess the minimal amounts of injected pilot fuel required which ensures a stable ignition and combustion of the lean premixed gas-mixture. Work is carried out in close collaboration with the Laboratory of Combustion Engines of the University of Munich, in the framework of the co-funding project “Piloteinspritzung” of the German FVV.

Ignition of a homogeneous gas-mixture by injection of a small amount of liquid fuel (so-called pilot injection, which auto-ignites), is a complex process which is not fully understood and still largely optimized by „trial-and-error“ procedures. The auto-ignition sites of the diesel pilot spray droplets provide stable ignition sources for the lean air/gas charge. The whole combustion can conceptually be divided into three main phases, namely the auto-ignition of the pilot spray, a transition phase (development of a flame kernel) and the subsequent turbulent flame propagation in the premixed gas.

The main objective of work packages AP4b and AP2b is to carry out a detailed analysis of the main processes of ignition and combustion induced by pilot injections of liquid fuels. Therefore, in AP4b a systematic investigation of the ignition behavior and the following homogeneous flame propagation by means of a detailed analysis of the reaction kinetics is necessary which is then supported and validated with the experimental results from AP2b.

4.1 Experimental setup

The main characteristics of the ETH single stroke machine are shown in Table 1.

bore	B=84 mm
stroke	s=120 – 250 mm
compression ratio ε	5 -30
piston bowl	d_{bowl}=52 mm, 4 mm depth
piston optical access	d_{window}=52 mm, quartz
cylinder pressure	p_{max} up to 200 bar
cylinder head	flat, highly flexible
pressure measurement system	piezoelectric pressure transducer (Kistler no. 7061B), pressure levels from 0 - 250 bar
heating	Cylinder head, cylinder liner and piston up to 400 K
injection system	flexible, multiple injectors possible
ignition system	spark plug possible, flexible
# of experiments	15-20 per hour

Table 1: characterristics of the ETH single stroke machine.

For safety reasons, the methane is injected directly into the cylinder by means of a Siemens hollow cone piezo injector which has seen successful application in previous studies for gaseous fuel injec-

tion into the single stroke machine in previous studies [3]. The methane injector was located 35 mm off-axis in the cylinder head, next to the centrally located common rail pilot injector (Figure 19). The piezo injector has an umbrella angle of 90 degrees and was operated with a needle lift of about 25 µm. The pilot injection of the diesel fuel was realized with a standard solenoid actuated BOSCH multi-stream injector.

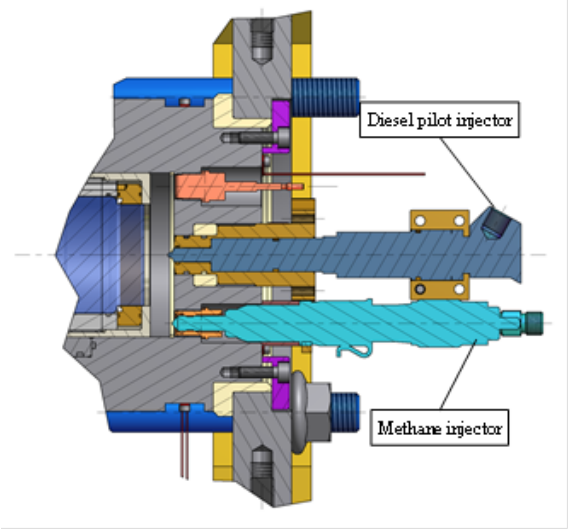

Figure 19: configuration of the two injectors in the cylinderhead.

Two different multistream nozzle tips on the pilot injector were used with an umbrella angle of 160 degrees, the production grade 6-hole orifice and a modified 3-hole orifice which was derived from the original nozzle tip by closing three holes (welding). The injected pilot mass was held constant with constant injection parameters for both nozzle tip geometries, while the amount of premixed methane was varied. A summary of the operating conditions for the single stroke machine and the injection parameters can be found in Table 2.

compression ratio ε	20 (p_i=1.2 bar, p_d=32.5 bar)
wall heating temperature	333 K
mean temperature before compression	330 K
cylinder head	flat, with two injectors
pilot ignition system	Bosch common-rail system, 2. Generation, IAV FI^{2re}
pilot fuel type	diesel (cetane number 51.7, density 834.1 kg/m^3)
pilot injection rail pressure	400 bar
start of pilot injection	4.1 ms bTDC (at 830 K, 30 bar in the cylinder)
pilot injection duration	0.25 ms (electrical), 0.33 ms (physical)
hydraulic injection delay	0.35 ms
total injected pilot mass 3-hole orifice (and standard deviation)	0.64 mg (σ=0.03 mg) per stroke
total injected pilot mass 6-hole orifice (and standard deviation)	0.85 mg (σ=0.04 mg) per stroke
hole diameter of pilot nozzle tip	0.152 mm
λ_{CH4}-variation	1.5-2.7
gaseous fuel	Methane
injection pressure Methane	50 bar

Table 2: operating parameters of the ETH single stroke machine.

The injection of the diesel pilot fuel for both nozzle tip configurations was analyzed with an injection rate analyzer from IAV, to obtain information about total injected mass, hydraulic injection delay and time resolved mass flow rate through the injector. For the applied injection parameters the total injected mass, its standard deviation and the hydraulic injection delay (averaged over 500 injections) can be found in Table 2.

Figure 20 shows exemplarily injection rate measurements for different injection pressures and the standard deviations.

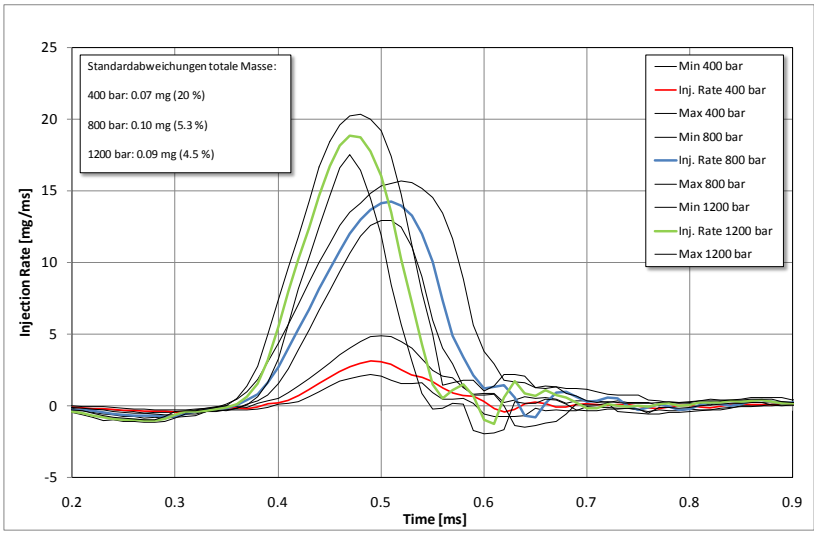

Figure 20: injection rate measurements for different injection pressures.

The pilot injection occurred at the same time for all measurements; a total amount of 0.64 mg for the 3-hole nozzle tip and 0.85 mg for the 6-hole nozzle tip was injected. Depending on the air to methane fuel ratio, this corresponds to between 0.8 and 1.8 percent of the total chemical energy in the system. The diesel pilot injection is controlled by IAV FI2re and is triggered at a specific piston position 4.1 ms bTDC which corresponds to the pressure and temperature condition at 25° CA bTDC at an engine speed of 1500 RPM in the test engine at LVK/TU Munich which is a modified single cylinder engine (MTU 396).

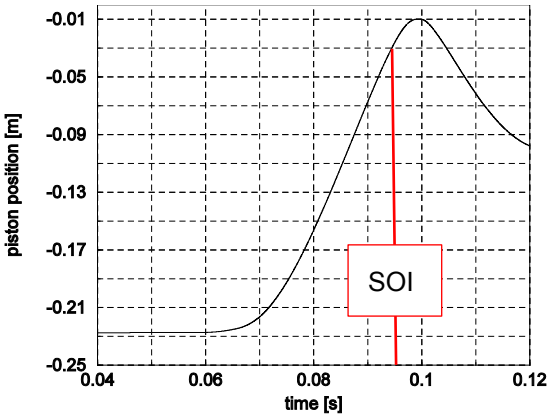

Figure 21: sample piston position trace for a compression stroke with the applied parameters without combustion.

To achieve a homogeneous mixture of the methane and air at the start of the pilot injection, the gaseous methane was injected early in the compression stroke, about 750 ms before TDC. Figure 21 shows an exemplary piston position trace without combustion for the applied operating conditions; the start of injection (SOI) for the pilot fuel is also illustrated.

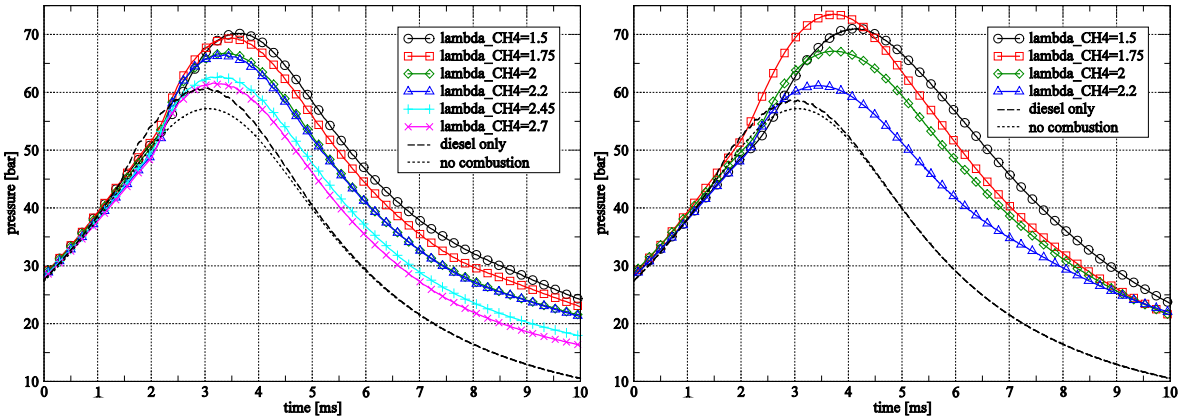

Figure 22: pressure traces for all investigated operating points for the 3-hole nozzle (left) and 6-hole nozzle (right). Source [4].

To determine the injected amount of methane in the combustion chamber, a control volume with a specified volume and temperature was mounted before the methane injector, where the pressure drop during an injection could be assessed. A map of injection pressures, injection durations and resulting injected methane masses was established for all investigated operating points of the campaign.

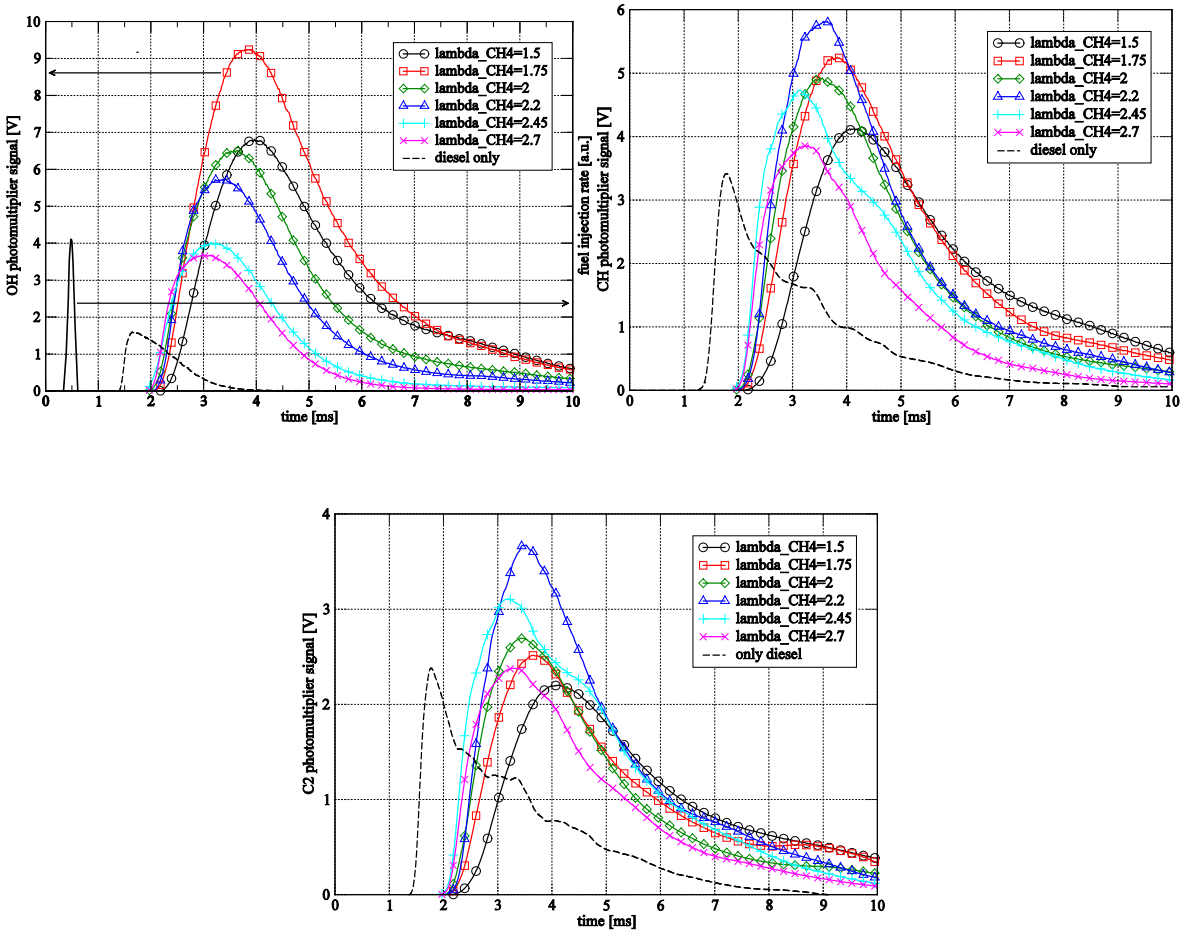

Figure 23: recorded photomultiplier signals for the 3-hole nozzle configuration with different λ_{CH4}, OH (top left), CH (top right) and C_2 (bottom). Source [4].

The optical accessibility through the piston window (d=52 mm, cf. Table 1) allowed for different optical measurement systems. An intensified high speed camera (LaVision HSS5) equipped with a 307 nm

band-pass filter recorded pictures of the OH chemiluminescence at a frequency of 10 kHz during ignition and combustion with a resolution of 512x512 pixels through the piston window. In addition, photomultiplier signals were recorded at a frequency of 100 kHz to acquire information concerning the total UV light emitted by the energized OH, CH and C_2 radicals.

Figure 22 shows the mean pressure traces (averaged over 5 strokes) for both nozzle configurations for various amounts of premixed methane. The peak pressure increases with the amount of premixed methane, as the amount of total energy is increased. The start of combustion and the peak pressure tends to be later with more methane in the ambient gas mixture. Diesel injection and combustion (black dashed line) in pure air shows a significantly earlier start of pressure rise than all other cases where methane is present in the ambient gas mixture.

Figure 23 shows the photomultiplier signals for all the operating points measured with the 3 ole nozzle configuration. As already observed before, diesel injection in pure air ignites much before every other case. Ignition delay seems to increase with the amount of premixed methane. The maximum of the photomultiplier signals is reached later with more premixed methane in the combustion chamber. For all the OH, CH and C_2 photomultiplier signals a longer signal is observed with increasing methane content which is an indication for longer combustion durations. For the extremely lean (in terms of methane) cases where no flame front propagation in the premixed mixture can be observed, the signal level is still significantly higher than for the case with pure air. The only exception to the rule that the photomultiplier signal levels rise with increasing methane content is the case with the lowest lambda (λ_{CH4}=1.5), this case was also the one with the longest ignition delay and the smallest slope of the signal. Two mechanisms are thought to be responsible for this counter trend behavior. First. with the longer ignition delay, there is more time for the pilot spray to mix with the surrounding methane/air-atmosphere. Second, this could lead to a lean premixed (auto ignited) combustion of the pilot spray and the entrained methane, which is both slower and less intense than combustion in stoichiometric regions.

Figure 24 shows the mean OH chemiluminescence images (averaged over 5 strokes) for both nozzle configurations for diesel combustion without methane present in the charge. Both cases with no methane present in the system for both nozzle tips show pure diffusion type combustion of the diesel pilot spray.

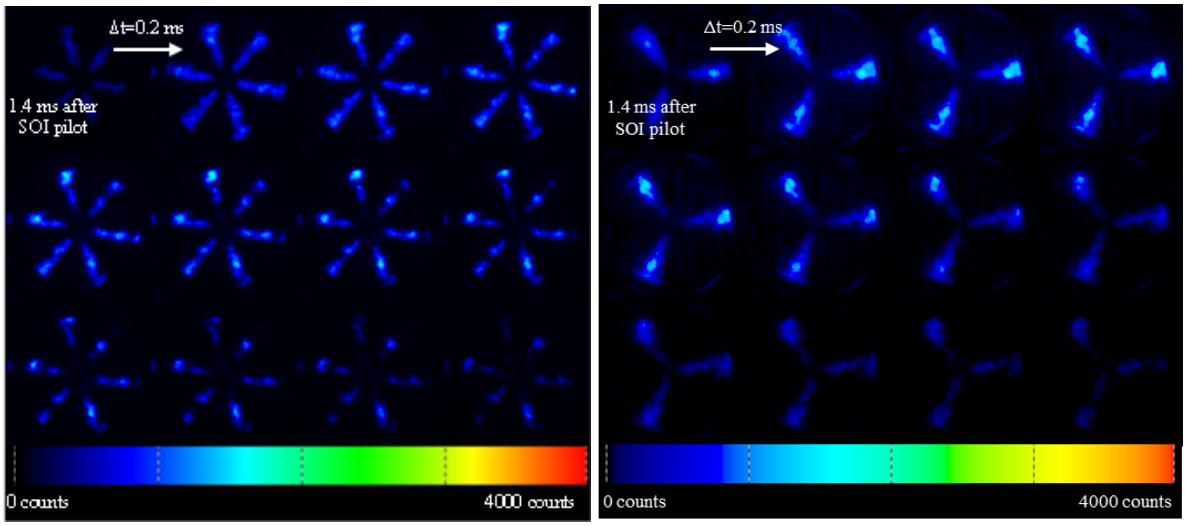

Figure 24: OH chemiluminescence images during ignition and combustion for the 6-hole (left) and the 3-hole (right) nozzle configuration for diesel combustion in air with no methane in the surrounding gas charge. Source [4].

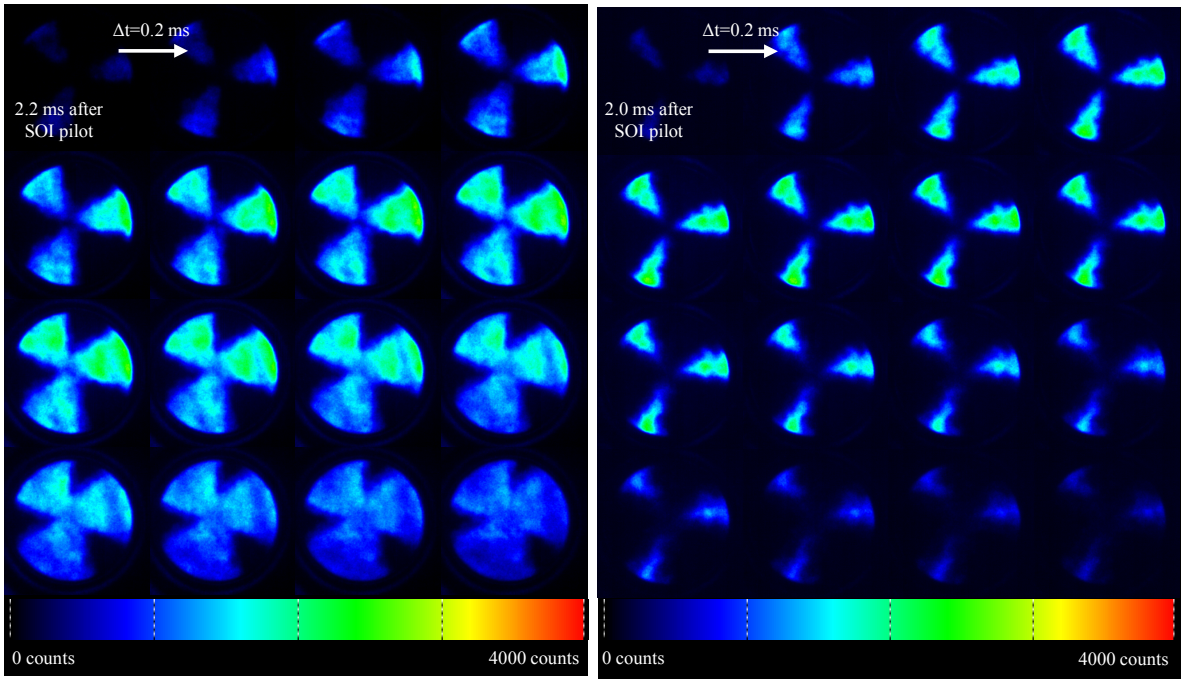

Figure 25: OH chemiluminescence images during ignition and combustion for the 3-hole nozzle configuration for an air excess ratio of the premixed methane/air charge of λ_{CH4}=1.5 (left) and λ_{CH4}=2.7 (right). Source [4].

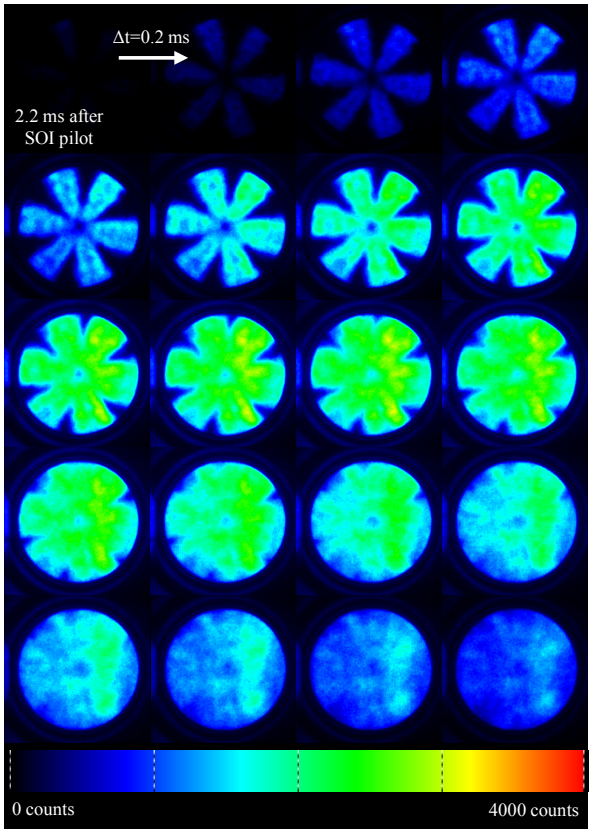

Figure 26: OH chemiluminescence images during ignition and combustion for the 6-hole nozzle configuration for an air excess ratio of the premixed methane/air charge of λ_{CH4}=1.5. Source [4].

OH chemiluminescence images for diesel in pure air and λ_{CH4}=2.7 for the 3-hole nozzle tip are shown in Figure 24 (right) and Figure 25 (right), respectively. Although there is very little methane present in the second case, the ignition delay is significantly longer than in the first case. The areas of high combustion intensity around the pilot spray cones are much wider than in the case without methane in

pure air. This can be attributed to the better mixing be-cause of a longer ignition delay and because the methane which is entrained in the pilot spray and in the close vicinity of the spray combustion burns as well, although under such lean conditions no flame propagation in the premixed charge can be sustained. This trend enhances with increasing amounts of premixed methane until flame propagation in the unburnt methane/air-mixture can take place for both nozzle configurations (Figure 25 left, Figure 26).

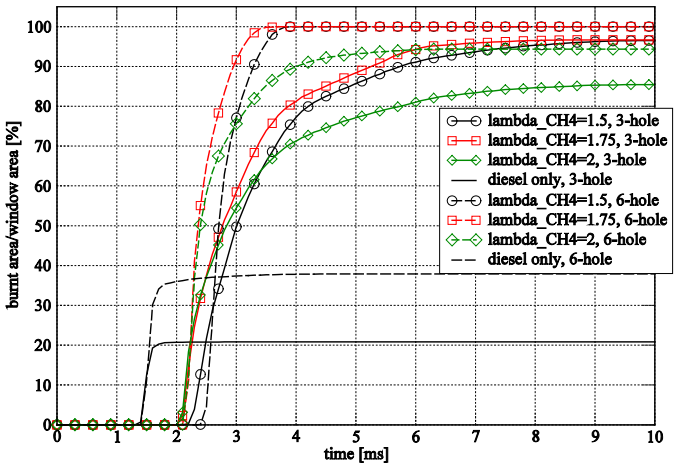

Figure 27: evolution of the burnt area/window area calculated from high speed OH images for both nozzle configurations by summing up all the pixels that ever had a signal. Source [4].

Figure 27 shows the evolution of burnt area over window area for different conditions. The traces were obtained by summing up all the pixels in the window area that ever had a signal. Comparison of the two cases for diesel in pure air shows a higher end value of about 40 percent for the 6-hole nozzle compared to the 3-hole tips where only about 20 percent of the visible area was covered by the flames. For a λ_{CH4} value of 2, flame propagation in the premixed region is very slow and some zones in the combustion chamber are never reached by the flames.

The 6-hole nozzle provides a much faster evolution of the flame area due to the doubling of ignitions spots and consequently the initial flame surface. The same behavior of the 6-hole nozzle compared to the 3-hole nozzle can be observed for the cases with λ_{CH4}=1.75 and λ_{CH4}=1.5, where faster flame propagation in the premixed charge takes place. The application of the 3-hole nozzle for the pilot spray, shows that the combustion never covers the whole window area, not even the case with λ_{CH4}=1.5. From these observations it can hence be concluded, that pilot injection using the 6-hole nozzle accelerates the combustion of the premixed charge considerably.

These experimental findings have been successfully published in [4] and presented at the SAE world congress in Detroit, MI on 25th April 2012.

In **AP4b**, a new 3D Computational Fluid Dynamic (CFD) model for the simulation of natural gas fuelled and diesel pilot ignited dual fuel combustion was developed. The different combustion regimes and fuels as well as their influences on each other are treated by coupling two combustion models. The Conditional Moment Closure (CMC) model described in more detail in chapter “5.1 Simulation platform” below, has been extended specifically toward dual fuel combustion. A detailed reaction mechanism for n-heptane from [5] has been used, which is able to describe the autoignition and combustion of the pilot spray in a methane containing atmosphere as was demonstrated in [6]. The spatial and time resolved ignition spots computed in the CMC code are handed over to the parallel running premixed combustion model as spark cells for the subsequent flame propagation in the unburnt methane air mixture.

Premixed combustion of the methane-air charge and flame propagation was modeled using the Weller model [7,8] for partially premixed regimes. It is a flame area model in which the wrinkling factor de-

scribes the flame surface together with a regress variable. The laminar flame speed is determined following the approach of Gülder [9].

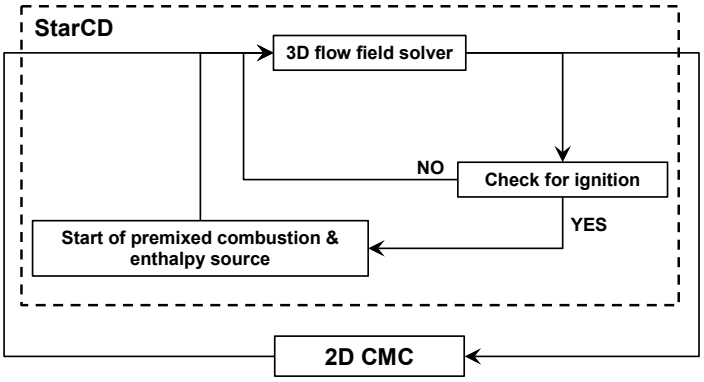

Figure 28: structure and working principle of the full CRFD model with the coupling. Source [10].

The hot spots computed by the CMC model serve as ignition sources for the premixed combustion model, a coupling through user coded subroutines was realized. A check for ignition is performed in every time-step and for every cell of the computational domain. If ignition in the CMC model has occurred, premixed combustion is started in these ignition cells together with an enthalpy source modeling the energy released by the ignition processes. Figure 28 shows schematically the structure and working principle of the full model.

In the coupled model, a threshold value of the OH concentration is employed to initiate the premixed combustion in the cells where ignition of the pilot spray has occurred (normally defined by a threshold of the conditional temperature of 1600 K in the CMC code). Since both the OH concentration and the temperature values show a strong "runaway" as soon as ignition starts (Figure 29), the onset of ignition is insensitive to the chosen threshold value.

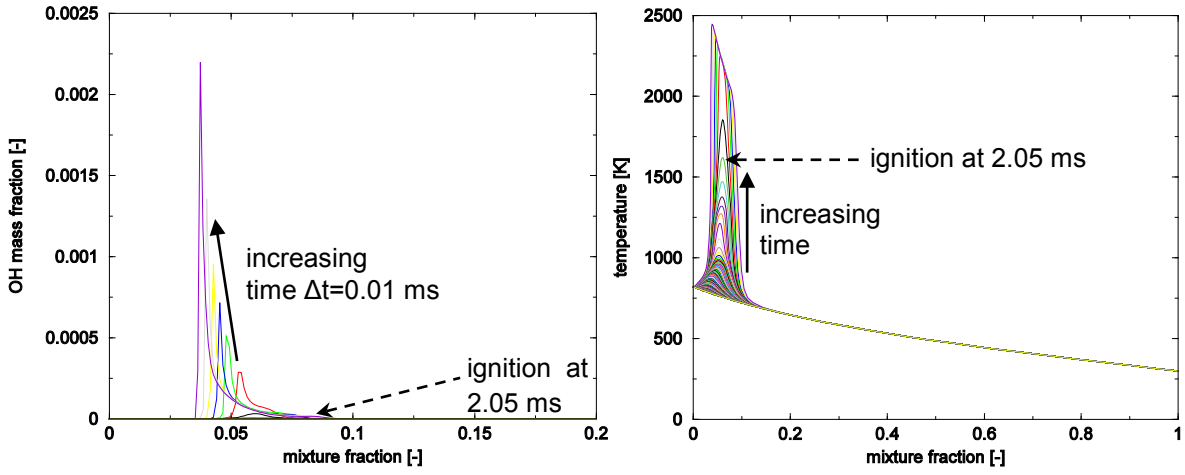

Figure 29: OH mass fraction (left) and temperature (right) runaway during ignition for CMC standalone computation starting from frozen mixing. Source [6].

Figure 29 shows the evolution of OH concentration (left) and the temperature (right) in the mixture fraction space computed with a stand-alone CMC simulation in a counterflow setup started with frozen mixing for λ_{CH4}=1.5 in the oxidizer stream, 820 K starting temperature on the oxidizer side and 300 K on the fuel side at a pressure of 30 bar. The conditional scalar dissipation rate $\langle N|\eta \rangle$ is modeled by means of amplitude mapping closure (AMC [11]) with a prescribed peak value $\langle N|\eta=0.5 \rangle$ of 5 s^{-1}.

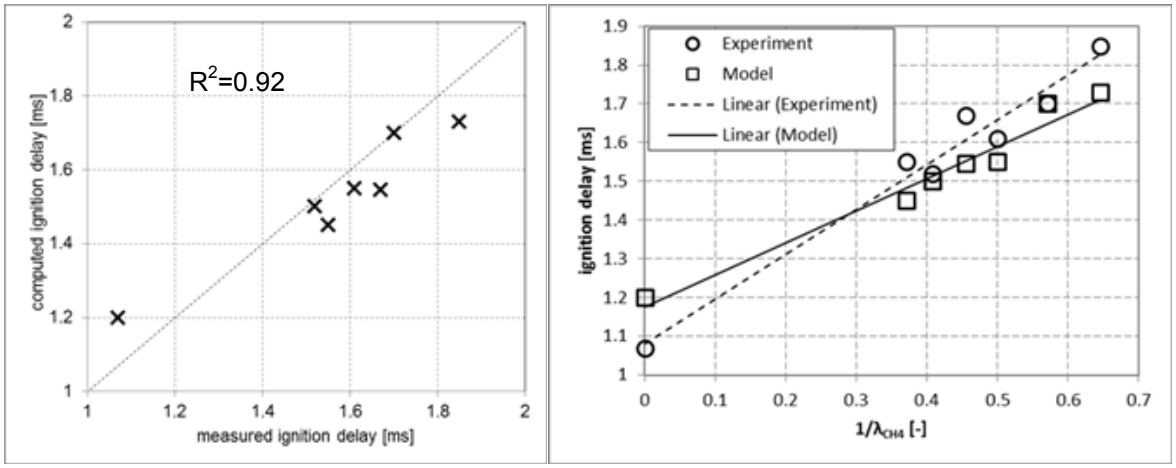

Figure 30: Comparison of computed and measured ignition delay for the 3-hole nozzle configuration, regression plot with correlation coefficient (left) and ignition delays with linear trendlines for various operating points (right). Source [6].

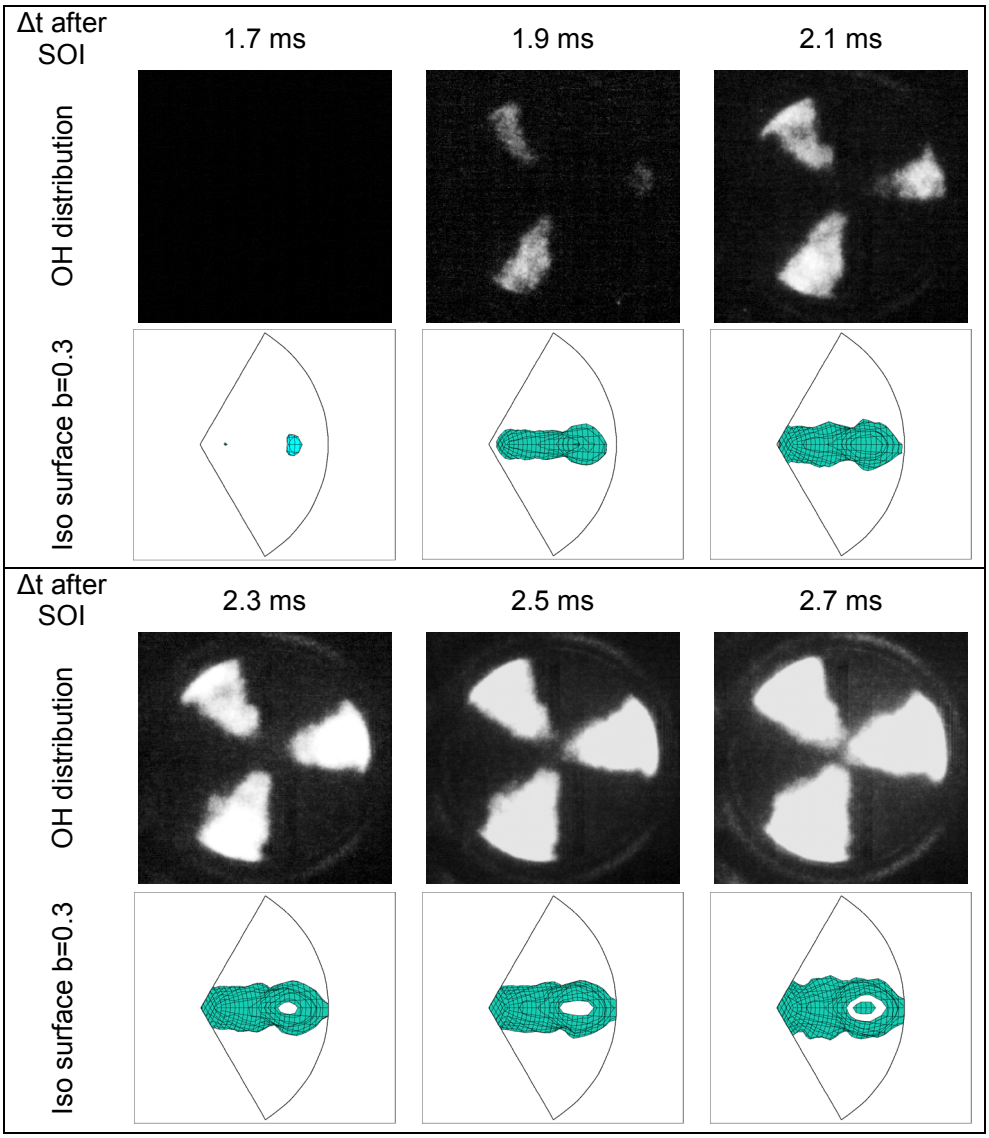

Figure 31: Evolution of the mean OH distribution and computed iso surface for b=0.3 for a λ_{CH4} value of 1.5. Source [6].

Figure 30 shows a comparison of the calculated versus the measured ignition delays for the 3-hole nozzle. The regression plot over all investigated operating points (Figure 30, left) shows good agreement between measured and calculated ignition delay times. The ignition delays increase with increasing amounts of methane (Figure 30, right), which is very well captured in the simulation, since the effect of the methane on the auto ignition of the pilot spray is taken into account by the application of a reaction mechanism for n-heptane oxidation with methane as a reactive component.

The 2D spatial OH chemiluminescence imaging data (line of sight along the cylinder axis direction through the window in the piston) provides time resolved information on the ignition location and subsequent combustion, allowing for comparison of the recorded images with the calculated iso-surface of the flame front. The latter is characterized by the change in the regress variable which changes from a value of 1.0 in the unburnt to 0 in the burnt gases at the flame front position. Figure 31 shows the evolution of the OH distribution and the iso-surface of the regress variable at a value of 0.3 for an air/fuel ratio of λ_{CH4}=1.5. The shape of the initial flame kernel is predicted well by the simulation and the propagation of the flames towards the injector location in the center is also well captured.

These developments have been successfully published in [6] and [10].

4.2 Conclusions

Important information concerning the nature of dual fuel combustion could be gained both from experimental as well as simulation work could be gained. The experiments showed an increasing ignition delay of the pilot spray with increasing amounts of methane in the surrounding atmosphere, which in the case for Lambda_CH4=1.5, where the longest ignition delay is observed, leads to a lean premixed ignition in the pilot spray. This lean premixed ignition showed lower levels of OH, CH and C2 chemiluminescence in the overall combustion than ignition and combustion with lambda_CH4=1.75 because the pilot spray had more time to mix with the surrounding gas. Furthermore, the application of the 6-hole injector for the pilot spray was seen to considerably speed up the combustion of the premixed gas charge compared to ignition with the 3-hole injector over a wide range of equivalence ratios.

The coupling of two different combustion models has proved to be a valuable approach to account for two different combustion modes as well as two fuels in the system and their influence on each other. The influence of methane in the base charge on the ignition delay of the pilot spray can be taken into account by application of a detailed reaction mechanism for n-heptane oxidation with methane as a reactive component. By coupling the two combustion models through user subroutines the computed ignition spots of the auto-ignition can be treated as ignition locations for the premixed combustion model varying in time and space. The coupled full model shows good agreement with the experimental data both in ignition delay times and location. The initial flame shapes are seen to be in good agreement over the whole range of operating conditions; however, during the later stages of the premixed combustion the simulation seems to underpredict the flame propagation. This issue needs further investigation and will be addressed in follow up projects.

4.3 Major achievements

Experiments with diesel spray pilot injection in a methane air mixture under various conditions have been performed on the ETH single stroke machine. Optical and transient data of the dual fuel combustion processes were acquired for different operating conditions. The successful application of the developed combustion model for dual fuel combustion could be shown. Excellent agreement of computed and experimentally obtained ignition delay times as well as ignition locations and initial flame shapes with respect to the amount of methane in the ambient gas mixture is observed. Future experimental campaigns in the follow-up projects is thought to provide further insight to the dual fuel combustion and deliver more experimental data for further development of the combustion model.

The co-funding FVV Project “Piloteinspritzung” has been successfully completed, the final report is documented in [12]. Proposals for follow-up project(s) “AGR” and “Miller/Atkinson” as well as the BfE-project “Aladdin” have been accepted and are currently well underway.

5 Work package AP3

Work package AP3 comprises model developments and validation by means of data from a variety of experimental facilities.

5.1 Simulation platform

The Conditional Moment Closure (CMC) combustion model employed belongs to the class of presumed probability density function (PDF) approaches, which has seen successful application to a broad range of non-premixed combustion set-ups. These include single-phase flames [13,14,15,16,17,18,19,20,21,22,23] and autoignition of jets [24,25,26,27,28] as well as sprays, [29,30]. The code is jointly developed in the framework an ongoing collaboration between LAV, ETH Zurich and the Engineering Department of Cambridge University, UK; funding is independently available at both institutions.

5.2 Numerical method

The full model consists on the one hand of a CFD flow field solver suitable for the description of turbulent, compressible, two-phase reactive flows; at LAV, the flow field solver STAR-CD [31] is employed, which is a commercially available CFD solver widely adopted in the engine combustion community. The flow field solver is fully two-way coupled to the Conditional Moment Closure (CMC) combustion code as is illustrated in Figure 32:

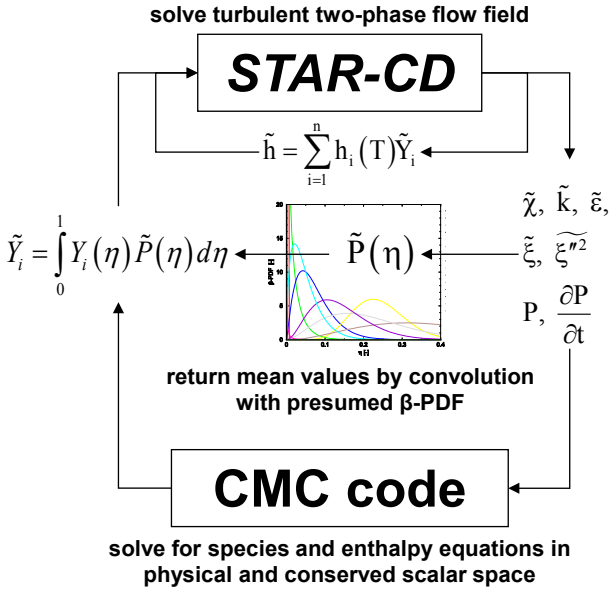

Figure 32: Schematic of the coupled combustion model consisting of multi-dimensional CMC code and CFD flow field solver. Source [32].

On the CFD solver side, two types of turbulence modeling are investigated: On the one hand, the governing equations are solved in a Reynolds Averaged Navier Stokes (RANS) context using the RNG variant of the k-ε turbulence model. Alternatively, Large Eddy Simulations (LES) are performed using a one-equation transport equation for the subgrid turbulent kinetic energy k_{sgs}. In both cases, standard model constants have been employed, for further information the reader is referred to [31].

The fuel spray is treated with a Lagrangian-Eulerian approach, where primary and secondary break-up are modeled using models available in STAR-CD, i.e. [33] and [34], respectively. For liquid droplets, thermo-physical properties of n-dodecane as a function of temperature have been adopted to repre-

sent the Diesel fuel used in the experiment as is common practice; for the experiments with n-heptane, the corresponding n-heptane droplet properties were used.

The CFD solver has been coupled with an elliptic first order CMC combustion model which is a presumed probability density function (PDF) method. For non-premixed combustion, the gas-phase mixture fraction is employed as conditional quantity. The governing equations are solved conditionally on mixture fraction for chemical species and temperature. The conditional expectations of the α-th species mass fraction, Q_α, and of the temperature, Q_T, denoted by:

$$Q_\alpha\left(\eta,\mathbf{x},t\right)=\left\langle Y_\alpha\left(\mathbf{x},t\right)\middle|\xi\left(\mathbf{x},t\right)=\eta\right\rangle \tag{1}$$

$$Q_T\left(\eta,\mathbf{x},t\right)=\left\langle T\left(\mathbf{x},t\right)\middle|\xi\left(\mathbf{x},t\right)=\eta\right\rangle \tag{2}$$

where $\left\langle \bullet\middle|\xi\left(\mathbf{x},t\right)=\eta\right\rangle$ represents ensemble averaging for the case that ξ fulfills the condition on the right side of the vertical bar. Assuming high Reynolds number and unity Lewis number, equations for conditional temperature and species mass fraction can be obtained. In the RANS context, these read as, following [35]:

$$\begin{aligned}\frac{\partial Q_T}{\partial t}+\left\langle u_i\middle|\eta\right\rangle\frac{\partial Q_T}{\partial x_i}=\left\langle N\middle|\eta\right\rangle\frac{\partial^2 Q_T}{\partial\eta^2}+\left\langle N\middle|\eta\right\rangle\left[\frac{1}{\left\langle c_P\middle|\eta\right\rangle}\left(\frac{\partial\left\langle c_P\middle|\eta\right\rangle}{\partial\eta}+\sum_{\alpha=1}^{N}\left\langle c_{P,\alpha}\middle|\eta\right\rangle\frac{\partial Q_\alpha}{\partial\eta}\right)\right]\frac{\partial Q_T}{\partial\eta}\\ -\frac{1}{\overline{\rho}\tilde{P}\left(\eta\right)}\frac{\partial}{\partial x_i}\left[\left\langle u_i''T''\middle|\eta\right\rangle\overline{\rho}\tilde{P}\left(\eta\right)\right]+\frac{1}{\left\langle c_P\middle|\eta\right\rangle}\left\langle\frac{1}{\rho}\frac{\partial P}{\partial t}\middle|\eta\right\rangle+\frac{\left\langle w_H\middle|\eta\right\rangle}{\left\langle\rho\middle|\eta\right\rangle\left\langle c_P\middle|\eta\right\rangle}\end{aligned} \tag{3}$$

$$\frac{\partial Q_\alpha}{\partial t}+\left\langle u_i\middle|\eta\right\rangle\frac{\partial Q_\alpha}{\partial x_i}-\left\langle N\middle|\eta\right\rangle\frac{\partial^2 Q_\alpha}{\partial\eta^2}+\frac{1}{\overline{\rho}\tilde{P}\left(\eta\right)}\frac{\partial}{\partial x_i}\left[\left\langle\rho u_i''Y_\alpha''\middle|\eta\right\rangle\tilde{P}\left(\eta\right)\right]=\left\langle w_\alpha\middle|\eta\right\rangle \tag{4}$$

Unclosed terms in the CMC equations are modeled using standard practice, i.e. using a linear correlation for the conditional velocities $\langle u_i|\eta\rangle$, a gradient flux assumption for the conditional turbulent fluxes and the AMC model [11] for the conditional scalar dissipation rate $\langle N|\eta\rangle$, for further details concerning the implementation and the interfacing of CFD and CMC codes the reader is referred to [36,37].

The conditional chemical source terms $\langle w_\alpha|\eta\rangle$ and $\langle w_T|\eta\rangle$ are closed at first order using different chemical mechanisms taken from the literature, depending on the set-up and conditions discussed in the respective chapters below.

The governing equations are discretized with a second-order central differencing scheme for the diffusion terms and an upwind scheme for convective terms. The mixture fraction domain is discretized into 101 nodes clustered around stoichiometry. As outlined in [35] and shown e.g. in [32], the resolution requirements in physical space for the conditional quantities are considerably lower, compared to their unconditional counterparts. Conditional expectations of species mass fractions and temperature have been initialized according to the adiabatic frozen mixing solution; i.e., linear distributions of species concentrations and enthalpy in mixture fraction space are assumed. Depending on the set-ups investigated, the oxidizer consists of technical air, in some cases dilution by EGR is considered; the fuel stream however always consists of pure fuel.

The unconditional species mass fractions required by the CFD code are computed by convolution of the conditional averages (obtained by the CMC code) with the presumed PDF. As a consequence, no transport equations for species are required in the CFD code. The mixture fraction PDF (a presumed beta function), requires the mean mixture fraction (eq. 5) and its variance (eq. 6), for which transport equations are solved:

$$\frac{\partial \overline{\rho}\tilde{\xi}}{\partial t} + \nabla\left[\overline{\rho}\tilde{u}_j\tilde{\xi} - \left(\overline{\rho}D_{\tilde{\xi}} + \frac{\mu_t}{Sc_{\tilde{\xi}}}\right)\nabla\tilde{\xi}\right] = \dot{S}_d \tag{5}$$

$$\frac{\partial \overline{\rho}\widetilde{\xi''^2}}{\partial t} + \nabla\left[\overline{\rho}\tilde{u}_j\widetilde{\xi''^2} - \left(\overline{\rho}D_{\widetilde{\xi''^2}} + \frac{\mu_t}{\mathrm{Sc}_{\widetilde{\xi''^2}}}\right)\nabla\widetilde{\xi''^2}\right] = \frac{2\mu_t}{\mathrm{Sc}_{\widetilde{\xi''^2}}}\left(\nabla\tilde{\xi}\right)^2 - \overline{\rho}\tilde{\chi} \tag{6}$$

where $\dot{S}_d$ accounts for droplet evaporation. $\tilde{\chi}$ denotes the unconditional scalar dissipation rate which is modeled using mean turbulence quantities as:

$$\tilde{\chi} = c_\chi \frac{\tilde{\varepsilon}}{\tilde{k}}\widetilde{\xi''^2} \tag{7}$$

where the model constant c_χ has been set to 2.0 as is common practice.

5.3 Model validation

Experimental data from four different optically accessible generic test rigs has been used for validation by means of 'high-fidelity' data, namely:

- The ETH combustion chamber "HTDZ" (cf. chapter 3.2, page 15)
- The Sandia closed combustion vessel
- Aachen constant pressure open flow reactor
- A "marine engine reference experiment", a constant volume spray combustion chamber (installed at Wärtsilä Switzerland, Ltd.) and the

All four of these test facilities are capable of high pressures and temperatures representative of conditions in Diesel engines at the start of fuel injection. The former three are of typical passenger car or truck engine sizes (with volumes of approximately one litre or less), while the marine test rig has a bore of 500 mm and a volume of roughly 30 litres, characteristic of large two-stroke marine engine combustion chambers at TDC.

In addition, data from a heavy-duty common-rail Diesel engine (Liebherr D924) installed at ETH has been used for model validation of full engine operation.

5.3.1 Liebherr D924 heavy-duty Diesel engine

At the early project stages during the commissioning of the MTU 396 single cylinder engine in AP1, existing data from an alternative engine was employed to benchmark the CMC code. Based on the first, highly encouraging results of the model when applied to a full engine configuration documented in [37], additional validation by means of heat release rate and NO_x emissions was performed for a wide range of operating conditions on a high quality measurement data-set from a heavy-duty engine which was recorded in the framework of a PhD Thesis at LAV [38].

The variations include on the one hand changes with respect to both the fuel path, i.e. different engine loads, RPM, injection timings and pressure and variations in the air path on the other.

5.3.1.1 Fuel path variations

The main engine data and the operating points investigated are summarised in Table 4 and Table 3, while the operating points investigated have been selected based on the European Steady Cycle test [39] conditions, for which an overview is given in Figure 56 in the Appendix.

operating point	load	engine RPM	start of injection [CA aTDC]	injection pressure [bar]
1	50%	1250	-4	1400
2	25%	1250	-3	520
3	25%	1250	-4	1400
4	25%	1250	0	1400
5	25%	1250	-4	1100
6	50%	1830	-4	1400
7	100%	1250	-4	1400
8	75%	1250	-7	800
9	100%	1250	0	1100

Table 3: Liebherr D924 heavy duty diesel engine: operating conditions corresponding to a selection of the European Steady Cycle test points.

Following a sensitivity study of the results with respect to CFD mesh dependence and CMC grid resolution/various dimensionality reduction strategies (not shown here), calculations were performed for all operating conditions listed in Table 3.

Heavy duty 4-stroke, direct injection, turbocharged, intercooled Diesel engine	
Cylinders	4
Bore	122 mm
Stroke	142 mm
Displacement	6.64 litres
Compression ratio	17.2
Crank radius / connecting rod length ratio	0.3114
Maximum boost pressure ratio	2.6
Maximum power output	183 kW
Engine top speed	2100 RPM
Maximum BMEP	20 bar
Maximum cylinder pressure	160 bar
Swirl (Tippelmann number)	0.65

Table 4: Liebherr D924 heavy duty diesel engine: main engine data.

As can be seen from Figure 33, Figure 34 and Figure 35 below, good agreement is reported with respect to the pressure traces and the heat release rates for the majority of investigated operating conditions.

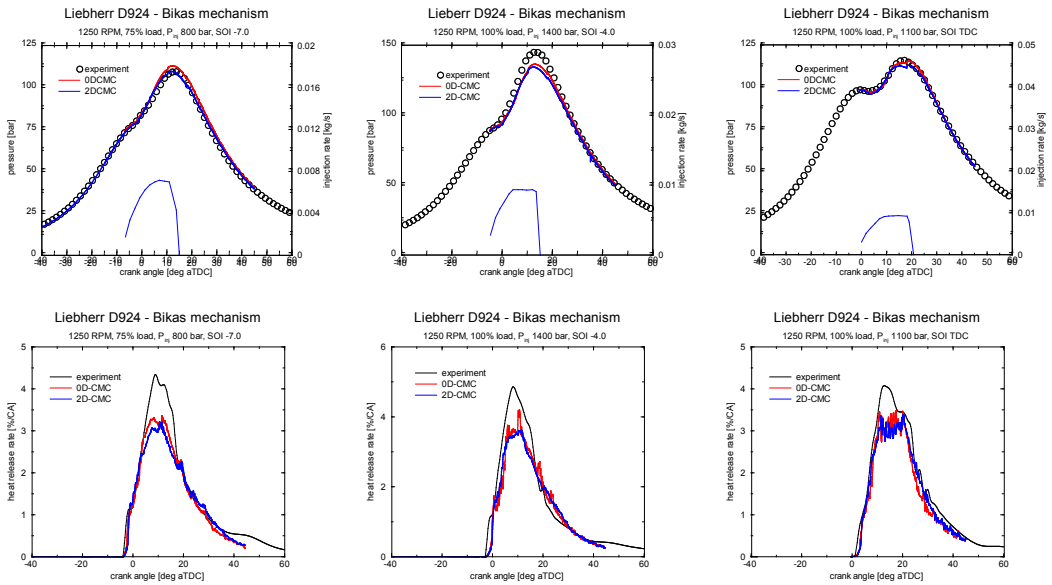

Figure 33: pressure traces (upper row, with superimposed fuel injection rates) and heat release rates (lower row) for 0D- and 2D-CMC approaches compared to the experimental data of the Liebherr D924 diesel engine for high load operating conditions. Source [32].

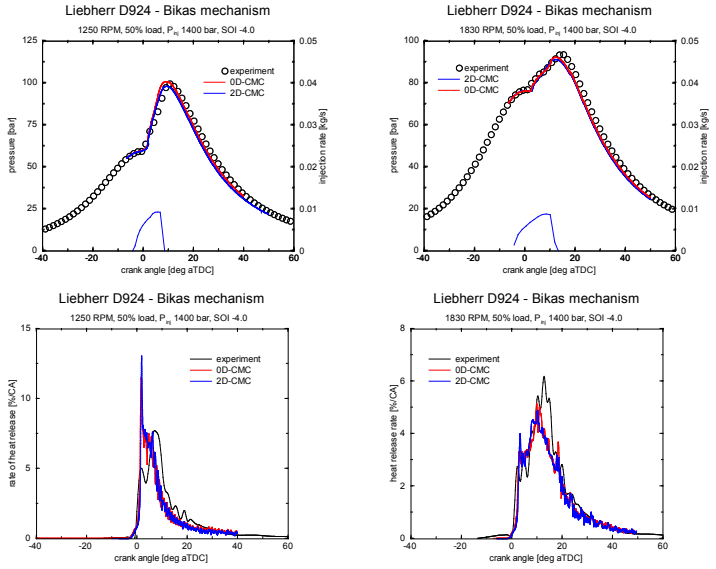

Figure 34: pressure traces (upper row, with superimposed fuel injection rates) and heat release rates (lower row) for 0D- and 2D-CMC approaches compared to the experimental data of the Liebherr D924 diesel engine for 50% LOAD operating conditions. Source [32].

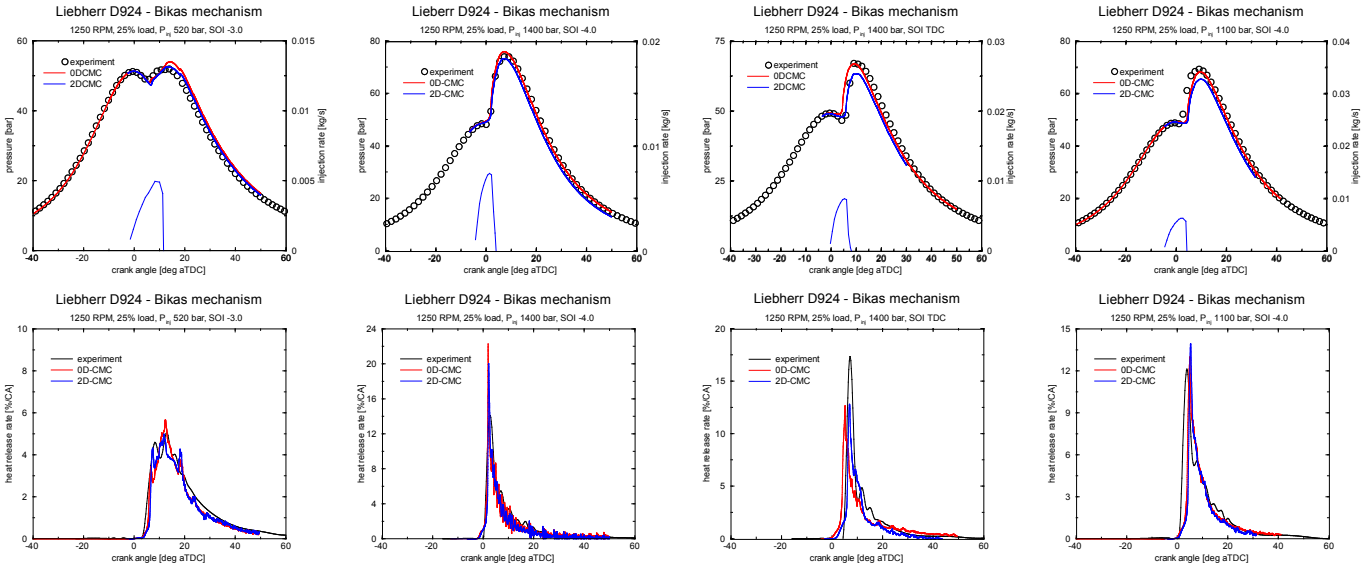

Figure 35: pressure traces (upper row, with superimposed fuel injection rates) and heat release rates (lower row) for 0D- and 2D-CMC approaches compared to the experimental data of the Liebherr D924 diesel engine for 25% LOAD operating conditions. Source [32].

The NO_x predictions are in fair agreement with the experimental data as is shown in Figure 36 below. While in absolute values, in some cases significant discrepancies can be observed compared to the experimental values, the trends are well captured:

- For the 50 percent loads, an increase in the engine speed is well predicted
- At 25 percent load, two trends are correctly represented, namely the increase in injection pressure for identical injection timing leading to higher engine out NO_x emissions as well as the influence of earlier injection timing for constant injection pressure showing increased NO_x levels.
- At full load, later injection leads to lower NO_x emissions.

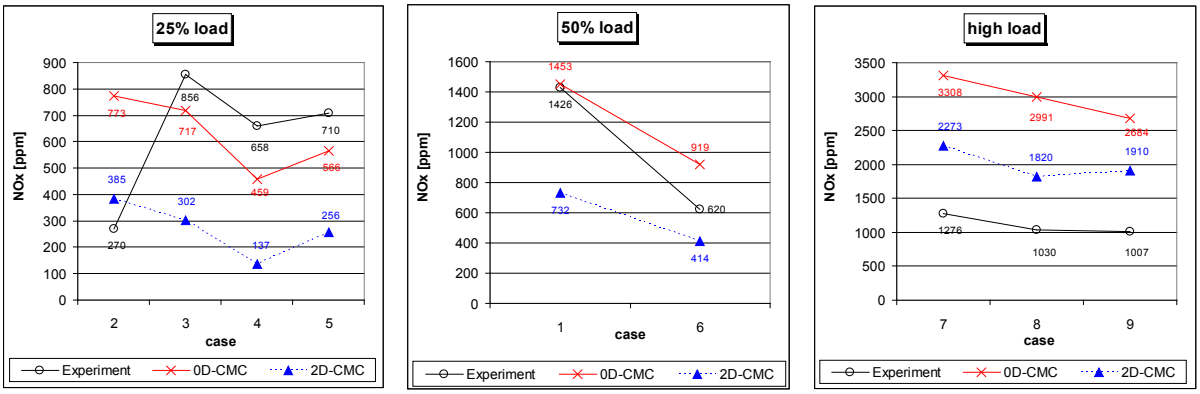

Figure 36: NO_x predictions For 0D- and 2D-CMC approaches compared to the experimental data of the Liebherr D924 diesel engine for a total of nine operating conditions at 25%, 50%, 75% and full load. Source [32].

These findings have been successfully published in [32].

5.3.1.2 Air path variations – influence of EGR

EGR is an important measure to reduce the NO_x emissions from Diesel engines. Since the cooled EGR module was not available on the MTU engine, additional data taken from [38] was employed also

for the validation of the CMC code to assess the predictions for varying inlet gas composition. Five different measurement points with four levels of EGR for a 25 percent load operating condition have been tested at an engine speed of 1250 RPM; the injection pressure was set at 1100 bar and the start of injection to 4 degrees crank angle before TDC.

A selection of results is presented below in Figure 37, showing reasonable agreement of the predicted pressure traces compared to the experimental data. As can be seen from the heat release rates; the ignition delay is over-predicted for the case without EGR, while for the 43 percent operating condition it is slightly under-predicted. For the latter, the peak heat release is also underestimated. As a consequence, the absolute values of the computed NO_x emissions are under-predicted for both conditions; the trend however is well captured.

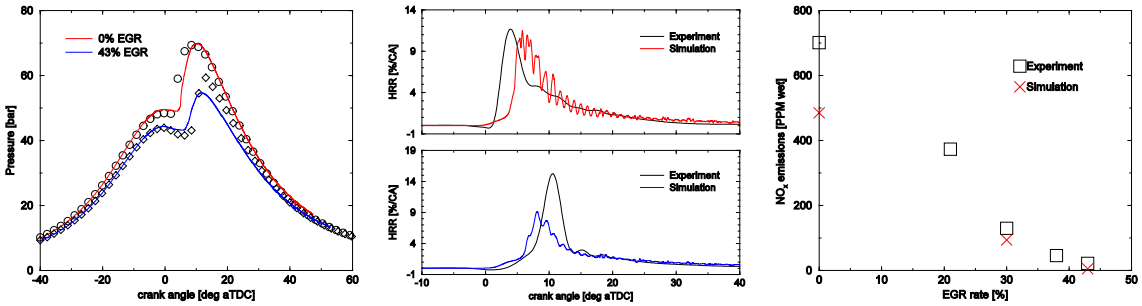

Figure 37 Heavy-duty truck engine: Influence of EGR on pressure traces (left, open symbols experiment, solid lines predictions), heat release rates (middle: upper 0% EGR, lower 43% EGR) and NO_x emissions (right). Source [40].

Both findings have been jointly shown in an invited presentation reviewing recent developments and application of CMC to two-phase configurations in [40].

Further efforts are envisioned for a broader data-set and will employ the emerging data from work package AP1 featuring controlled intake and exhaust conditions and, in addition, colder conditions due to Miller valve timing.

5.3.2 ETH high-pressure high-temperature test rig

A specific data-set has been generated by using n-heptane in lieu of Diesel in the ETH combustion chamber described in detail in chapter 3.2. The measurement details are summarized in Table 5 below.

The excellent optical access enabled the acquisition of Mie scattered light enabling validation of the dense core and shadow images for gas phase penetration length validations. Furthermore, pressure was recorded for the validation of the predicted energy conversion during the combustion event and chemiluminescence images provided information concerning the ignition location; additional information can be found in [41].

While the ignition delays and pressure rise were seen to be highly reproducible for a large number of experimental realizations, the ignition delay exhibits a large scatter, as is evident from Figure 57 and Figure 58 in the Appendix.

Two sets of investigations were carried out: On the one hand, the CMC combustion model was employed in a RANS turbulence model context to assess the sensitivities of the model with respect to a) the chemical mechanism employed, b) the atomization model and c) the measurement uncertainties with respect to temperature and turbulence levels at the time of injection. Secondly, an LES formulation of the flow field solver and CMC equations was used to investigate the capability of the code to capture variation in the individual event and hence predict scatter in the time and location of ignition and the early stages of combustion.

Fuel type	n-Heptane
Injection pressure	320 bar
Injection duration	1.80 ms (electrical) 1.65 ms (physical)
Total injected fuel mass	~4.7 mg
Nozzle diameter	0.15 mm
Nozzle L/D	4
Air pressure	80 bar
Air temperature	776 K
Wall temperatures	~800 K

Table 5: Operating conditions for the ETH high pressure high temperature cell.

5.3.2.1 RANS-CMC sensitivity analysis

In a first step, two chemical mechanisms have been compared. Although the oxidation of *n*-heptane is among the best known chemistries (for engine relevant spray combustion conditions), substantial discrepancies were seen concerning the ignition delays and subsequent pressure rise. To assess the temperature influence, simulations have further been performed at 10 and 20 K lower temperatures from the nominal measured value of 776 K, which correspond to a measurement inaccuracy of roughly 1.5 and 3 percent. Large differences can be observed in Figure 38 which compares the pressure traces of the experiment and five different simulation results.

For comparison with the simulation data, the mean ignition location averaged from the individual realisations (see Figure 58 in the Appendix) have further been compared, which are given in Figure 39.

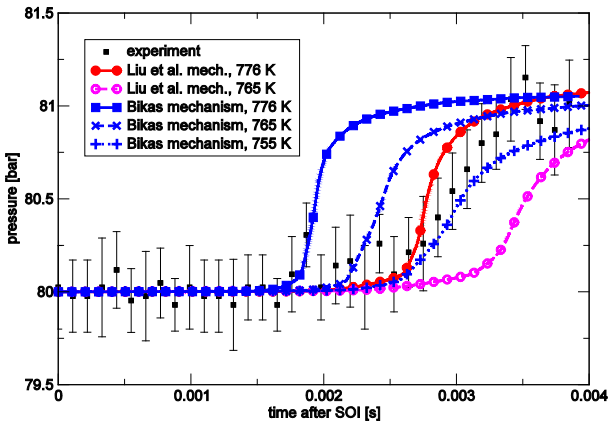

Figure 38: Pressure variation with time for various initial air temperatures and two chemical mechanisms [5,42]. Source [41].

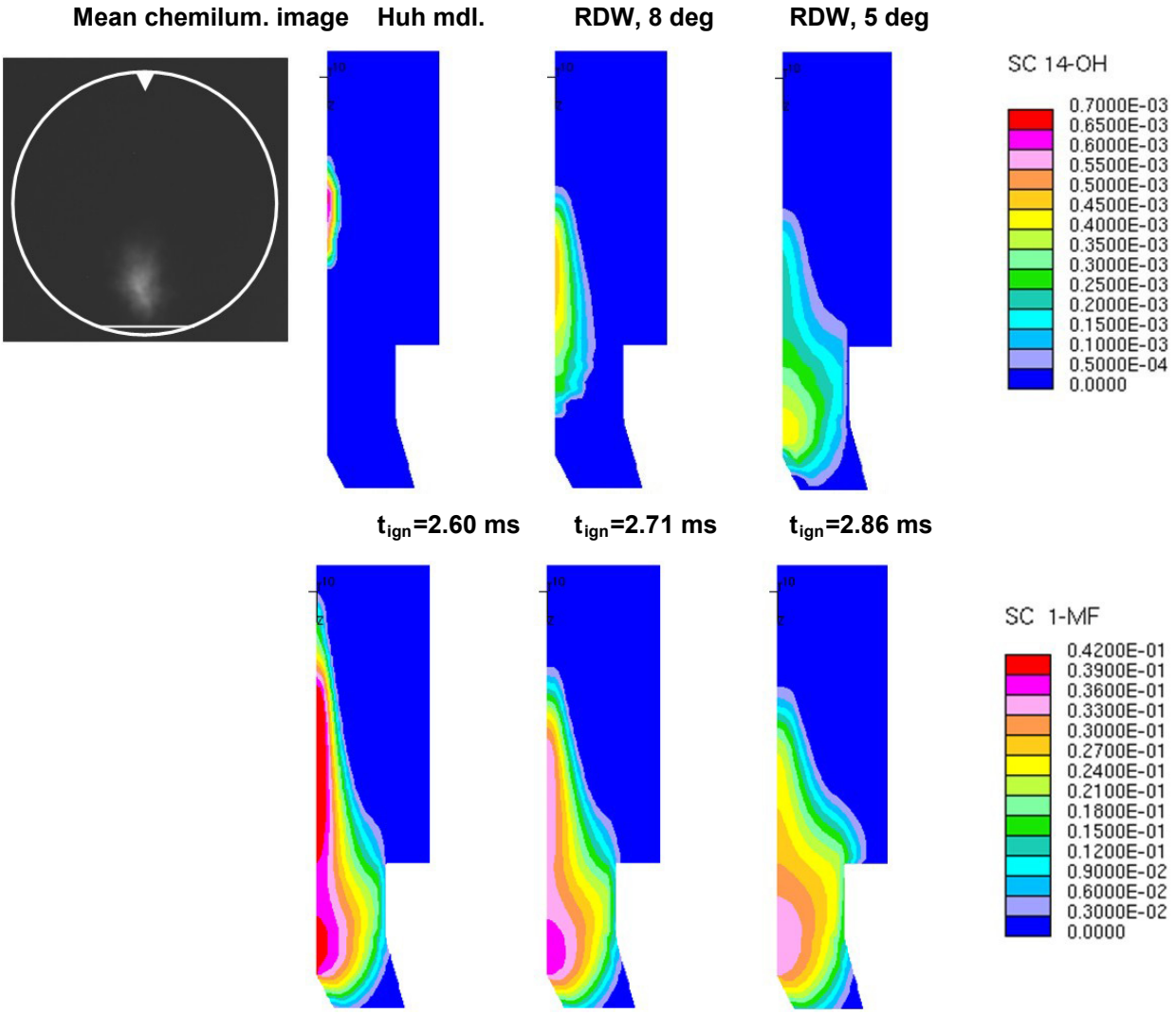

Figure 39: Ignition location comparison: Mean OH* chemiluminescence signal averaged from 48 individual realisations 2.5 ms after start of injection (upper left); the white circle symbolises the cell window, the straight line at the bottom the location of the wall and the triangle the injector. Simulated OH mass fraction (upper row) and mixture fraction (lower row) iso-contours at the time of ignition for two different atomization models: Huh model [33], the Reitz-Diwakar Model [34] with 8 and 5 degrees cone angle (from left to right). The Liu et al. mechanism [5] has been used at the nominal air temperature of 776 K. Source [41].

It can be concluded, that the influence of the chemistries and uncertainties in the initial temperature measurements can have a comparable influence on the ignition delay predictions. The choice of atomisation model prescribed cone angle show only minor impact on the ignition time and pressure rise, the ignition location is however strongly affected. In cases where the location of the flame is important, e.g. in case of engine combustion with substantial heat losses due to 'cold' walls, these finding indicate that spray atomization plays a major role and could have a similar influence on the heat release rate prediction as the choice of the chemical mechanism.

These findings have been successfully published in [41].

5.3.2.2 LES-CMC: Towards predicting the stochasticity of auto-ignition

RANS-CMC simulation techniques provide ensemble averaged results which can readily be compared to results which have been averaged from a large number of experimental realisations (cf. preceeding chapters).

Initial flow fields from individual cycles of internal combustion engines however have been seen to exhibit substantial variations between cycles [43,44]. In addition, the high pressure fuel injection

events are not perfectly repeatable, resulting in strong variability from cycle-to-cycle of the turbulent spray plume evolution and ensuing ignition event.

Even in the absence of substantial background flow field motion, e.g. at almost quiescent conditions in well-defined test rigs, large differences have been reported concerning the ignition locations [41] (cf. also Figure 58 in the Appendix). To compare individual injection and ignition events, an LES-CMC formulation based on developments from [45,46] was employed to assess the capability of the code to predict stochasticity due to the turbulent nature of the flow.

To assess the predictions, the early pressure rise has been compared with the experimental data as shown in Figure 40. The predictions are well within the experimental error bars. The lower spread of the predictions can be expected, since no numerical perturbation of the injection event has been employed and perfectly identical flow fields (velocities, turbulence and temperature) are initialised as well.

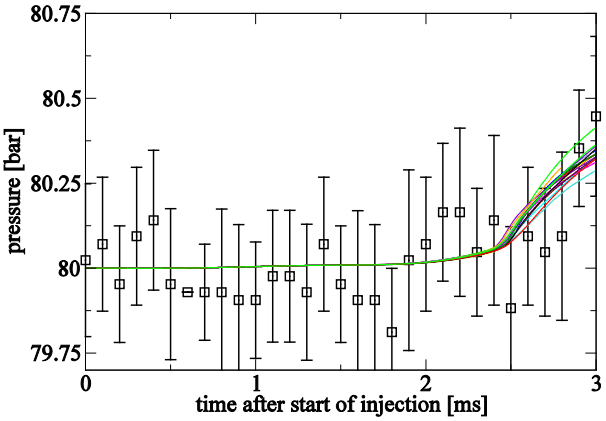

Figure 40: ETH bomb: Pressure evolution comparison during autoignition and early pressure rise. Experiment black squares with error bars, solid colour lines various computations using LES-CMC.

First results comparing ignition location predictions for the conditions summarised in Table 5 are presented in Figure 41. To obtain the location of ignition numerically, the peak temperature has been tracked for five different thresholds (1200 to 2000 K at 200 K intervals) in the observable domain. A wide range of ignition locations is predicted as can be seen from the scatterplot in Figure 41.

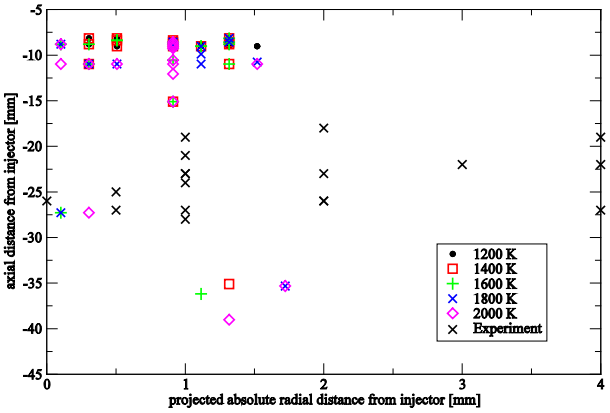

Figure 41: ETH bomb: scatter-plot of ignition location based on 5 different temperature thresholds for 18 predictions compared to experiment.

The average distance of the ignition spots from the injector location has been calculated from the experimental data from [41] and using all threshold values to assess the sensitivity of the predictions. For the recorded pictures, the radial distance was not easy to determine as the image obtained was a 2D projection of the 3D distribution (the experiment is a line of sight method). For the predictions, the

absolute values of the Cartesian X components have hence been used for comparison. Figure 42 shows the predicted ignition locations hereby obtained together with the experimental values. As can be observed, the predicted locations of autoignition are close to 0.9 mm from the axis for all temperature thresholds with standard deviations between 0.4 and 0.53 mm. Axially, the computed values range between 8.7 and 14.5 mm downstream (in negative Z direction from the injector), since higher thresholds ignite further downstream most likely due to transport of heat and radicals in the flow direction. The experimental locations are farther from the injector both axially and transversally and exhibit substantially higher variation in the radial position, while the standard deviation axially is smaller compared to all thresholds from 1400 K up. A smaller spread compared to the experiment is observed in the simulations and the results show a great sensitivity in how the autoignition spot is defined.

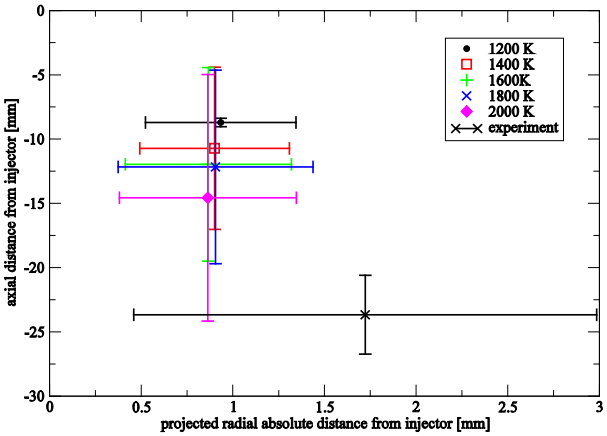

Figure 42: ETH bomb: averages and standard deviation of ignition location based on 5 different temperature thresholds for 18 predictions compared to experiment.

Note that the autoignition location determined from the experiment involves significant uncertainties, as it is based on the centroid of images of flamelets *after* autoignition has occurred. Since the flow is mainly in one direction, it is expected that the estimated autoignition location from the experimental flame images will be shifted downstream compared to the true autoignition location, and so the accuracy of the LES-CMC prediction is better than what is implied in Figure 42.

Publication of these recent findings is currently in preparation.

5.3.3 Aachen high-pressure high-temperature open chamber

The same LES-CMC code has been used to investigate the onset of ignition for a wide range of temperatures. The set-up assessed is a constant pressure high temperature flow reactor, for which RANS-CMC simulations have been reported previously in [36] and the experimental data is taken from [47].

Motivated by considerations put forward in [30] following the first application of LES-CMC to spray combustion at engine-like conditions, in this investigation a broad range of temperatures has been studied to assess the predictive capability of the LES-CMC code with respect to changes in the ambient conditions. Ten calculations have been carried out for each temperature where identical initial fields have been initialized, i.e. perfectly uniform in temperature, including the near-wall region which is heated. Turbulence quantities are set to values estimated from experimental data, i.e. k_{sgs} = 10 m^2/s^2. Since the system is open, at the inflow boundary identical values have been prescribed, i.e. no synthetic inflow turbulence has been used. In the experiment [47], photomultiplier signals were recorded by means of three optical light probes in the UV and visible light range from which ignition delay times could be deduced, however little detail is given with respect to the employed thresholds for defining ignition. Therefore, different criteria to detect the numerical autoignition delay time have been used and the influence on the predictions studied. Since the system is open, pressure equilibrates and no pressure rise can be used as in e.g. [30]. The rate of change of the pressure signal (dP/dt) has hence been chosen as a possible candidate to detect ignition. Alternatively, the evolution

of the field total of OH can be employed. Figure 43 shows an example of the evolution of the volume averaged dP/dt (upper) and pressure signals (middle) plus the field totals of OH (lower) for the 823 K temperature. Both criteria produce similar autoignition times.

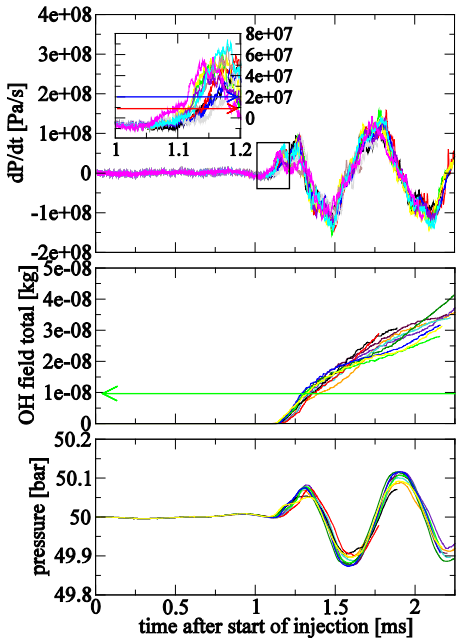

Figure 43: Aachen bomb 823 K: Predicted time evolutions for 10 calculations of the volume averaged rate of change of pressure (upper), volume averaged pressure (lower), OH field total (middle). The three thresholds assessed for the numerical ignition delay are indicated in red and blue for the rate of change of pressure (dP/dt=1.0 and 2.0x10^{+7} Pa/s, respectively), and green for the OH field total (1.0x10^{-8} [kg]), respectively.

To compare the ignition delay predictions with the experimental data, two thresholds of 1.0x10^{+7} and 2.0x10^{+7} [Pa/s] have been chosen for the dP/dt and for the OH a value of 1.0x10^{-8} [kg] is employed; for the former two, to simplify readability, the temperatures are offset by +/- 2 K in Figure 44, respectively.

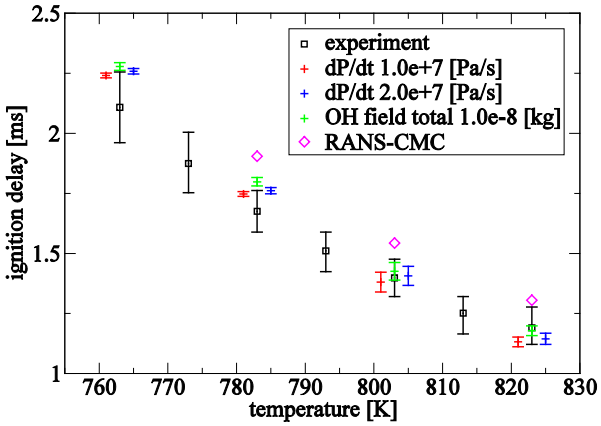

Figure 44: Aachen bomb setup: Ignition delay predictions for two thresholds of the rate of change of pressure of 1.0x10^{+7} and 2.0x10^{+7} [Pa/s], and for a field total of OH of 1.0x10^{-8} [kg] compared to experimental data; temperatures for the dP/dt predictions are offset by +/- 2 K for readability. RANS-CMC results are taken from [36].

As can be seen in Figure 44, the temperature influence is well captured for the broad range of temperatures relevant for Diesel engine combustion, with the ensemble-average autoignition delay time being close to the experiment. A smaller spread in the delay is predicted by LES-CMC compared to the experiment. This is not surprising, since the flow fields are initialised perfectly identically in all

simulations, i.e. no spatial variation of temperature or turbulence quantities was prescribed and since the small fluctuations of the injection timing and injection mass flow rates in the experiment have not been accounted for.

Publication of these recent findings is currently in preparation.

5.3.4 Sandia high-pressure high-temperature combustion chamber

Data documented in the open literature and available from the Engine Combustion Network [48] have been used for additional code validation. The test rig is a closed chamber of the constant volume type with an almost cubic shape with a dimension of roughly 100 mm and features excellent optical access.

This data has been selected since it provides additional information compared to the previously investigated high-fidelity test rigs. This includes in addition to ignition delay in particular lift-off lengths as well as soot volume fraction distributions for various oxygen contents at two chamber pressures.

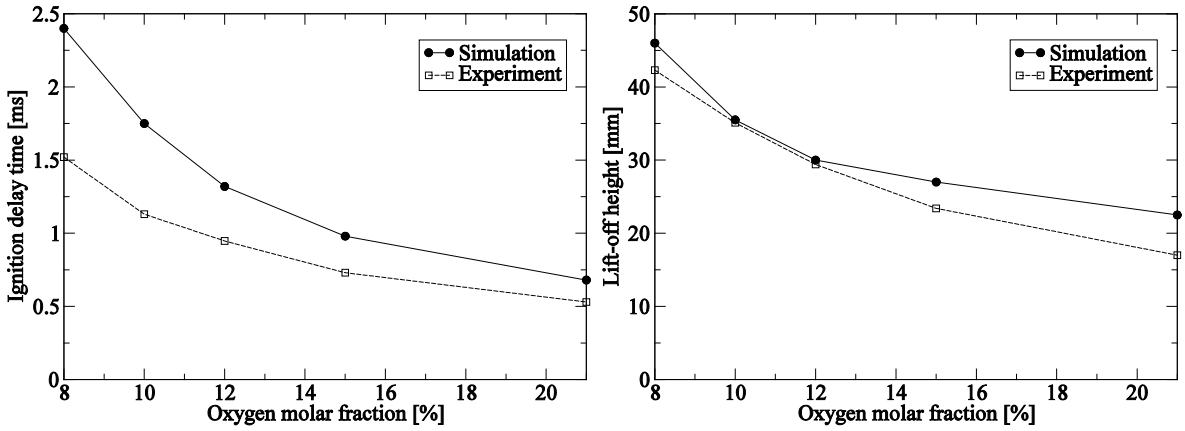

Figure 45: Ignition delay time (left) and lift-off length (right) for 1000 K and approximately 42 bar with different oxygen concentrations. Source [49].

Figure 45 shows ignition delays and flame lift-off lengths for different ambient oxygen concentrations, which represent the effect of dilution with recirculated exhaust gas 42 bar and 1000 K gas pressure and temperature, respectively. The ignition delay time is slightly over-predicted, however the trend with respect to the oxidizer concentration was captured correctly. The flame lift-off height can be considered in good agreement with the measurements.

The influence of EGR on the flame structure is presented in Figure 46 for the 21% and 10% O_2 cases. The corresponding stoichiometric mixture fractions amount to ξ_{ST}=0.061 and 0.0304, respectively. At the lower oxygen concentration, a broader flame can be seen with considerably lower temperature, acetylene and OH concentrations.

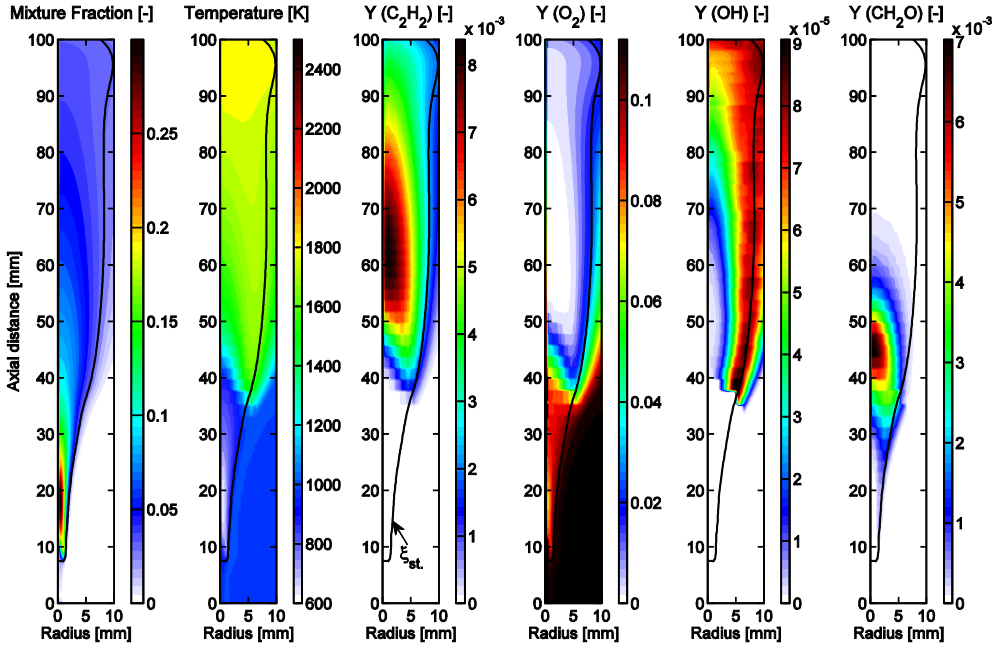

(a) 10% O_2, 14.8 kg/m^3, 5 ms after SOI

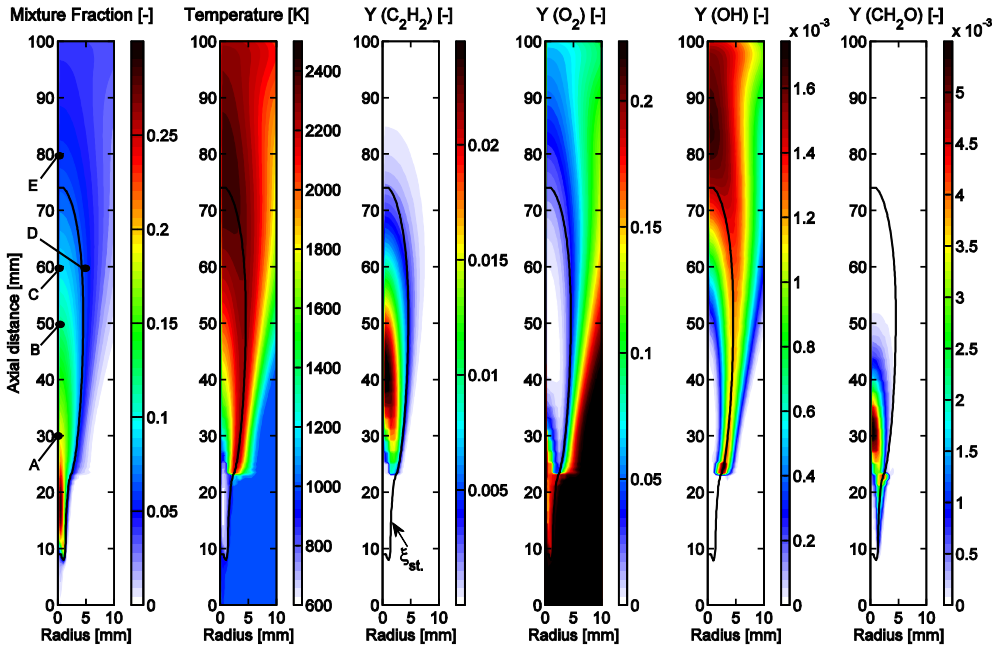

(b) 21% O_2, 14.8 kg/m^3, 5 ms after SOI

Figure 46: Spatial distribution of relevant quantities for flame characterization after 5 ms after SOI for two different ambient oxygen concentrations: (a) 10% and (b) 21% O_2. From left to right: mean mixture fraction, temperature, acetylene, oxygen, OH and formaldehyde. Source [49].

A two-equation soot model proposed by Leung [50] was integrated into the CMC framework towards predicting soot emissions. The distribution of the soot volume fraction two cases above is given in Figure 47. The location of the high soot concentration is well reproduced by the model, while absolute values are over-predicted in both cases. Nonetheless, for the total of nine cases from [49] (at two different ambient pressures and five ambient oxygen concentrations), semi-quantitative distributions have been reported.

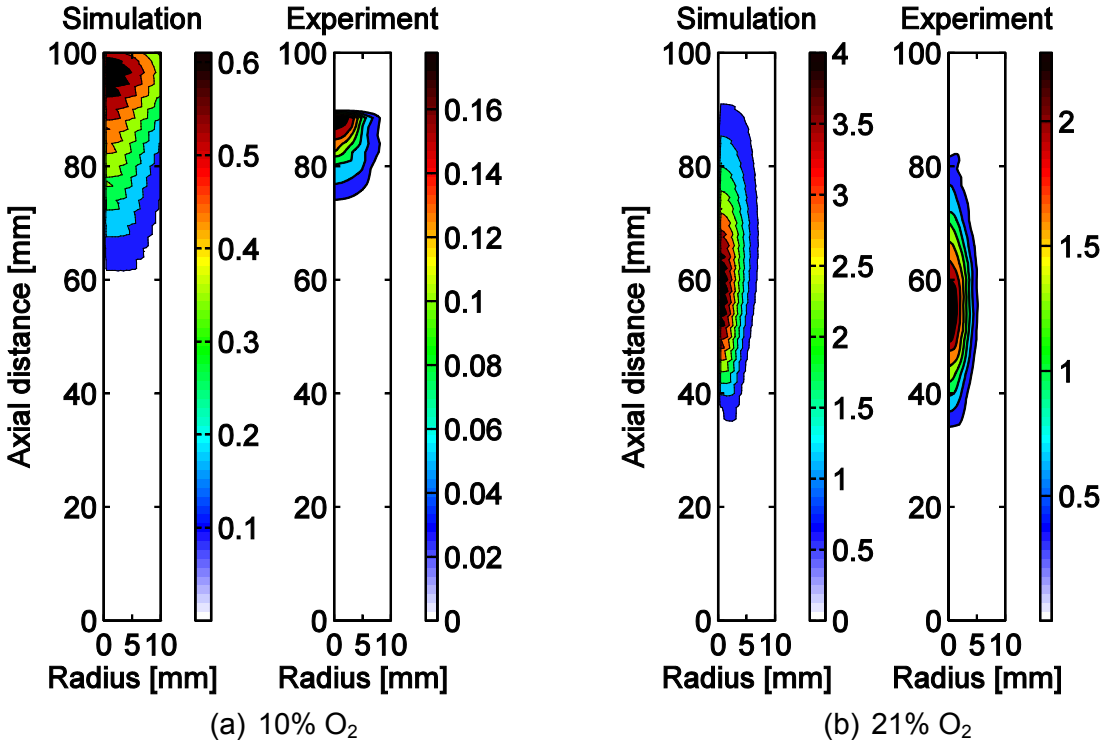

Figure 47: Comparison of spatial soot volume fraction (in ppmv) distribution 5 ms after SOI for 10% O_2 (a) and 21% O_2 (b). Source [49].

A detailed analysis of the spray flame characteristics in comparison with the conceptual model by [51] and soot model activities in the CMC framework have been submitted for publication [49] and presented in [52,53].

Based on these findings, it can be concluded that the model is capable of predicting a broad variety of physical processes present in auto-igniting fuel sprays at a wide range of conditions with no changes to model constants.

5.3.5 Large two-stroke marine Diesel reference experiment

To further assess the model at the dimensions and time-scales of large two-stroke marine engines, data from a spray combustion chamber (SCC) has been employed. This optically accessible marine Diesel engine reference experiment represents the combustion chamber of a large two-stroke marine engine at TDC (500 mm combustion chamber diameter), and is several orders of magnitude larger than the previously investigated set-ups; the characteristic time scales of the combustion event are also roughly one order of magnitude longer (25 ms injection duration). Further details concerning the experimental set-up can be found in [54,55].

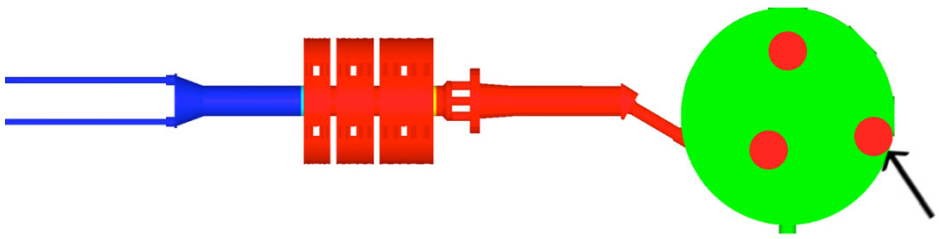

Figure 48: Spray Combustion Chamber numerical domain consisting of inlet (blue), regenerator and flange (red) and combustion chamber (green). The arrow indicates the location and direction of fuel injector. Source [56].

The SCC geometry is illustrated in Figure 48. The entire CFD grid consists of 1.25 million cells. In the combustion chamber (green) a hexahedral mesh is employed and the region relevant for the spray,

first 400 mm axially and 50 mm radially from the injector, has a perfectly hexahedral grid of 2 mm. Furthermore, the first 150 mm axially and 25 mm radially have been refined to 1 mm since grid sensitivity has been reported previously in [57] at non-reactive conditions. The spray penetration length and cone angles have been validated at a broad range of conditions, which include changes in air density and temperature.

Initialization of the flow field temperature, pressure, velocity, turbulent kinetic energy and turbulence dissipation rate at the start of injection (SOI) employs results from previous 'blow-down' simulations [54,58]. The flow exhibits strong swirling motion in the combustion chamber and corresponds roughly to a solid body rotation with a circumferential velocity of 20 m/s at 200 mm radius. Standard non-slip walls with wall-functions is employed to treat heat transfer (with a constant-temperature boundary condition, T_{wall}=453 K).

5.3.5.1 Spray modeling

A large number of non-reactive simulations have been performed and published at the ASME 2012 conference [56]. These include simulations of light Diesel fuel and heavy fuel oil (HFO) under non- and evaporating conditions (400 and 900 K) for three different ambient densities: 11, 22 and 33 kg/m^3. A grid sensitivity analysis has been carried out with three different mesh resolutions (1, 2 and 4 mm), in order to quantify the mesh dependence. The 2 mm (approximately twice the orifice diameter) grid was found to best fit with the experimental data [59] with respect to penetration length under non-evaporating conditions. This requirement in terms of mesh resolution, i.e. cell sizes of twice the injector diameter is qualitatively in agreement with previous studies reporting sensitivities of spray morphology evolution with comparatively smaller injector sizes [57].

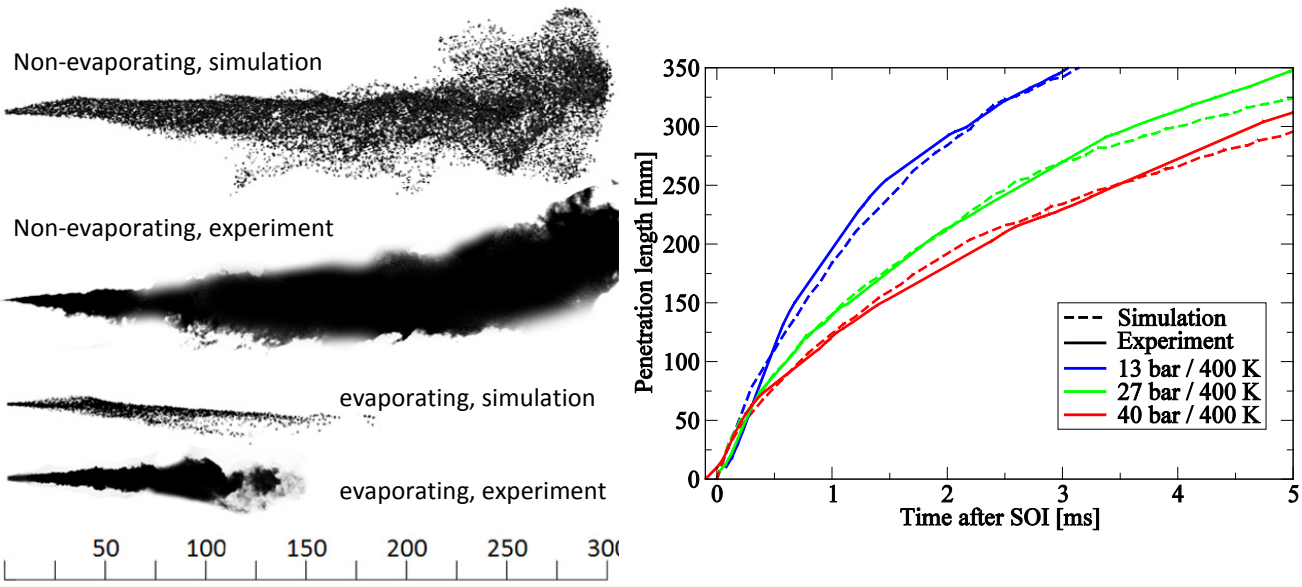

Figure 49: Simulated and measured spray shadow images under non- and evaporating conditions with 33 kg/m^3 (left); Spray penetration length under non-evaporating conditions for three different ambient densities (right). Source [56].

Figure 49 (b) shows the comparison of spray tip penetration for three different ambient pressures, where good agreement with experimental data is achieved. Figure 49 (a) illustrates the morphology of the simulated and measured spray under non- and evaporating conditions. The model reproduces well the shape of the spray with its characteristic lateral deviation due to the swirling flow present in the combustion chamber. The effect of evaporation is also captured, where the fuel has evaporated completely after approximately 150 mm from the injector tip.

5.3.5.2 *Combustion modeling*

Reactive calculations have been performed for the above set-up for a wide range of temperatures with constant density to ensure identical momentum exchange between the liquid and gas phases. As a consequence, the pressure needs to be adjusted; Table 6 provides an overview of the conditions investigated.

Case	Gas density [kg/m^3]	Gas temperature [K]	Gas pressure [bar]
1	33	910	91
2	33	790	79
3	33	760	76
4	33	730	73

Table 6: List of test cases considered for large marine engine reference experiment reactive calculations

The experimental ignition delay was determined through chemiluminescence appearance [60], corresponding to high temperature regions. Therefore in the simulation, the ignition delay is defined as the time after SOI when the maximal Favre averaged temperature first exceeds the arbitrary threshold value of 1600 K as applied by [41]. In the case of 21 % oxygen concentration, this definition was found to have a low sensitivity. As shown in Figure 50, the ignition delay was well reproduced for the large range of temperatures for which the ignition delays vary by one order of magnitude.

The computed ignition delay times are slightly overpredicted for all cases apart from the 910 K case and quantitatively the discrepancy was within 9 and 23 percent, whereas the standard deviation of the experimental values amounts to between 8 and 18 percent.

In addition to ignition delays, the ignition location has also been compared, which is defined as the axial distance from the injector where the temperature first exceeds 1600 K. Analogous to the time, the ignition distance increases substantially by diminishing the ambient temperature as illustrated in Figure 51 (lower).

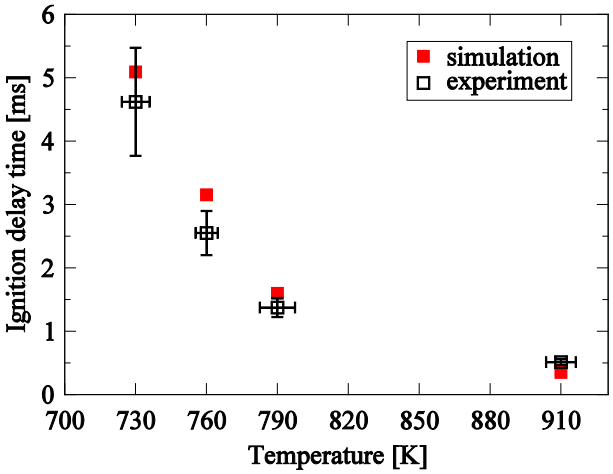

Figure 50: Ignition delay for different ambient temperatures. Source [61].

The simulation is capable to capture this trend well. The sensitivity of the location is high especially at the lower temperatures as was seen in [60], where it was further reported that once first ignition occurs, the spray ignites in a good portion of the spray within one image frame (62.5 µs).

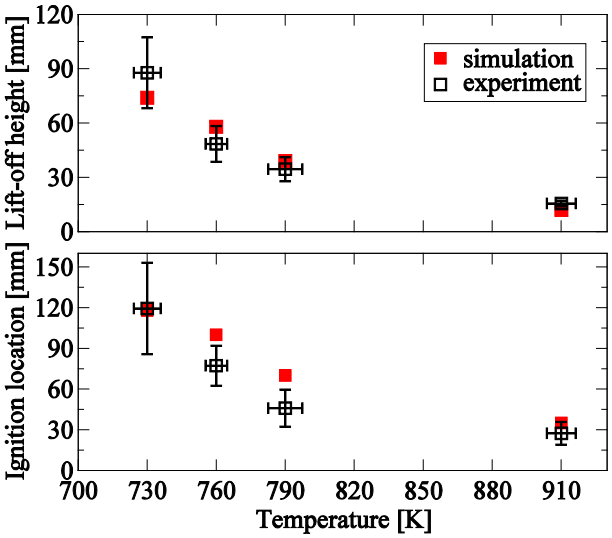

Figure 51: Ignition location (lower) and lift-off length (upper) as a function of ambient temperature. Source [61].

Figure 52 presents the computed ignition sequence by means of temperature isocontours for the test case at 760 K. The black lines represent the stoichiometry mixture fraction isoline (ξ_{st}). In agreement with the experiment, in all test cases ignition takes place on the right side of the spray due to the swirl motion. The effect of increased radial distance of the ignition location from the injector axis with reduced temperature is also captured (not shown here).

After ignition the flame quickly propagates upstream along the stoichiometric mixture fraction and subsequently stabilizes at a statistically steady distance from the injector, the so-called lift-off length, for which a comparison is shown in Figure 51 (upper). The simulation reproduces the correct trend and the quantitative values are within the experimental standard deviation. In the last decades various theories have been proposed to explain the mechanism of flame lift-off stabilization consisting mainly of extinction, propagation and triple flame theory as reviewed by [62] for gaseous jets and by [63] for Diesel jets.

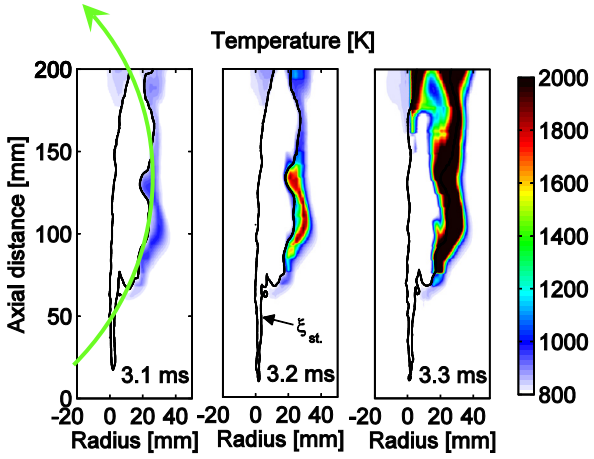

Figure 52: Temperature isosurface evolution at the time of ignition for the 760 K case (times in ms after SOI, ξ_{st} denotes the stoichiometric mixture fraction isoline and the green arrow indicates the swirl direction). Source [6156].

These findings have been accepted for publication at the upcoming COMODIA conference [61].

5.4 Conclusions and outlook

Data from a variety of different high-fidelity generic test rigs and engines have been used to validate the CMC combustion model and model developments have been carried out enabling soot emission

predictions. The experimental data includes variations in both the fuel path (SOI, injection pressure) as well as the air path (temperatures, pressure and EGR levels) and validation is performed using ignition delay and location (including the randomness thereof), pressure traces and heat release rates as well as soot mixture fraction distributions and engine-out NO_x emissions. Based on the good qualitative and quantitative agreement of the predictions for this broad range of conditions, it can be concluded that the CMC model is capable of representing a broad range of physics of auto-igniting fuel sprays. While sensitivity was found concerning the chemical mechanism employed, the CMC model shows good agreement without any tuning of model constants from case to case and can hence be considered predictive – with very few exceptions at least qualitatively, in many cases even quantitatively.

Future developments will focus on additional validation by means of optical engine data as well as the improvement of emission predictions. While the present soot model was developed and validated by means of on n-heptane measurements, the use of Diesel presents substantial additional challenges due to the presence of cyclic and aromatic fuel components affecting considerably the soot formation process. As a consequence, the assessment of alternative mechanisms for Diesel surrogates, comprising in addition more comprehensive soot precursor formation chemistry will constitute the next steps in model development. Validation will be carried out by means of data from both optically accessible test rigs as well as engines for a broad range of conditions.

5.5 Brief summary of major achievements

- First two-phase engine multidimensional CMC model presented in [37] and further validation for a broad range of conditions including heat release rates and NOx predictions in [**Error! ookmark not defined.**].
- Sensitivity analyses with respect to chemical mechanism, uncertainties in initial conditions and atomization models presented in [41].
- The development of a two-equation soot model in the CMC framework and first application to two-phase soot predictions have been proposed in [49].
- First application of CMC to large bore marine engine reference experiment is documented in [61].
- First investigations towards two-phase LES-CMC to capture the stochasticity of ignition events have been presented in this report and are currently in preparation.

5.6 Collaborations

In addition to the on-going collaboration with the University of Cambridge, valuable collaborations have been established in the framework of the Engine Combustion Network (ECN); in particular with Argonne National Laboratory, Politecnico die Milano and DLR.

Co-funding has been provided by the CCEM project “CeLaDe”, with additional co-funding for the large marine engine reference experiment is provided by the EU FP7 projects HERCULES-B and has lead to the establishment of the follow-up project HERCULES-C; all of which are gratefully acknowledged.

6 Work package AP4a

As part of AP4a, injection and in-cylinder pressure measurements from a medium speed diesel engine have been used to study Ignition Delay (ID) as a function of in-cylinder conditions during injection. The test engine used for the measurements is a Wärtsilä 6L20 Common Rail, which has a maximum output of 1080 kW at a nominal engine speed of 1000 RPM. The engine is part of the CCEM-LERF engine test-bed, located in PSI, Villigen, and is part of the CCEM - CELaDE project. More information about the engine test-bed can be found in [64] and [65].

The present study mainly concentrates around the effects of in-cylinder pressure and temperature during the injection period and before ignition to the ID. The test engine is equipped with a prototype two-stage turbocharging system, and has been run with different inlet valve timings to study the effect

of Miller cycle on combustion and emissions. The different valve timings have allowed the study of ID at a wide range of in-cylinder temperatures during injection. All measurements have been conducted with the same diesel fuel, which has a Cetane number of 51.

In a previous study using the LERF engine measurements, reported in June 2010, a single Arrhenius ignition model, tuned using the engine measurements, was used. In continuation of this experimental study of ID, a further investigation is ongoing, using more complicated models for ignition. In this investigation the same LERF engine data are used to study the applicability and performance of more advanced ignition models to large DI diesel engines.

6.1 Measurement points

To date 70 points have been studied. These cover a wide range of temperatures (740-930 K) and pressures (35-155 bar) which result from constant engine speed (1000 RPM) measurements at different loads and different inlet valve closure timings (increasing load at constant valve timing results in higher TDC pressure with unchanged TDC temperature due to constant inlet temperature from intercooling). All measurement points and their respective average temperatures and pressures during ID are plotted in the graph below:

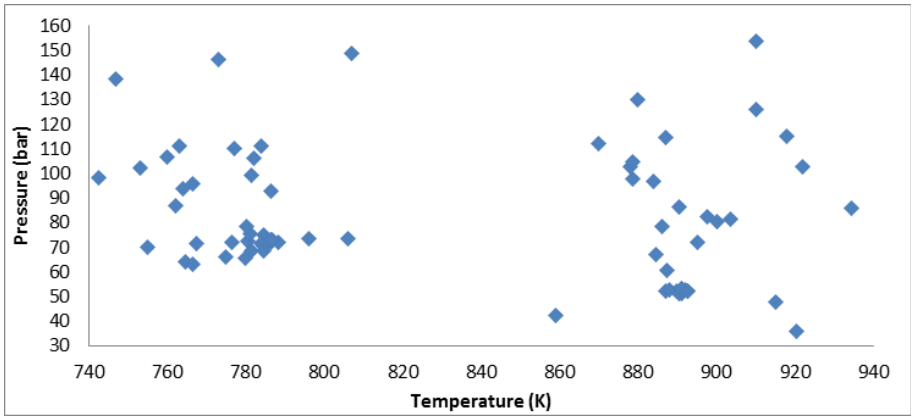

Figure 53: Measurement points shown with their respective average temperatures and pressures during ID.

6.2 The 3-Arrhenius ignition delay model

For the ID model, in place of the single Arrhenius approximation of ID presented in the previous report, a more accurate 3-Arrhenious expression was used, which has been shown to better capture the fuel chemistry behavior. In this model, low, medium and high temperature chemistry are accounted for separately, with the resulting ID calculation being a function of all three combined. The 3-Arrhenius ignition model used in this study has been developed as part of the BfE project 101,514 [66]. Further details about the model and the model calibration can be found in the aforementioned project report, or alternatively in [67].

In the 3-Arrhenius model, as was the case for the single-Arrhenius model, the ID is calculated for each case as a function of the time-dependent in-cylinder pressure and temperature. Additionally to these, the equivalence ratio and concentrations of N_2 and O_2 are used as parameters for the calculations.

All model constants have been calibrated using shock tube data, for fuels with similar cetane number as the fuel used in the LERF experiments (50). For the current investigation, all model constants were kept unchanged from their originally calibrated values.

The only parameter which was varied is the equivalence ratio, since there was no *a priori* information on a constant value for equivalence ratio for a DI engine. This issue arises from the fact that the models are calibrated using shock tube data and are developed for HCCI engines, where equivalence ratio is (assumed, and for all practical purposes) spatially constant. In the DI diesel engine case, equiva-

lence ratio is spatially and temporally variable, and thus is not relevant for a global 0-D ID calculation model.

6.3 Model ID prediction results

For the purposes of this study, a constant value of equivalence ratio was used as a representative value for all measurements. The value for equivalence ratio was treated as a variable, and ranged from 1 to 0.45. The resulting predictions of ID for all equivalence ratios studied are plotted against the measured ID values the in the graphs below:

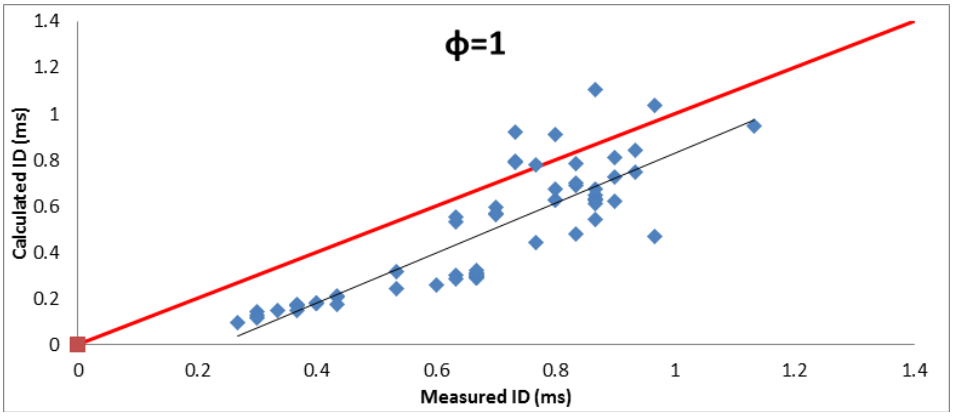

Figure 54: Calculated versus measured ignition delays (ID) for stoichiometric equivalence ratio (φ=1). The red line denotes a perfect agreement and the blue line the model predictions.

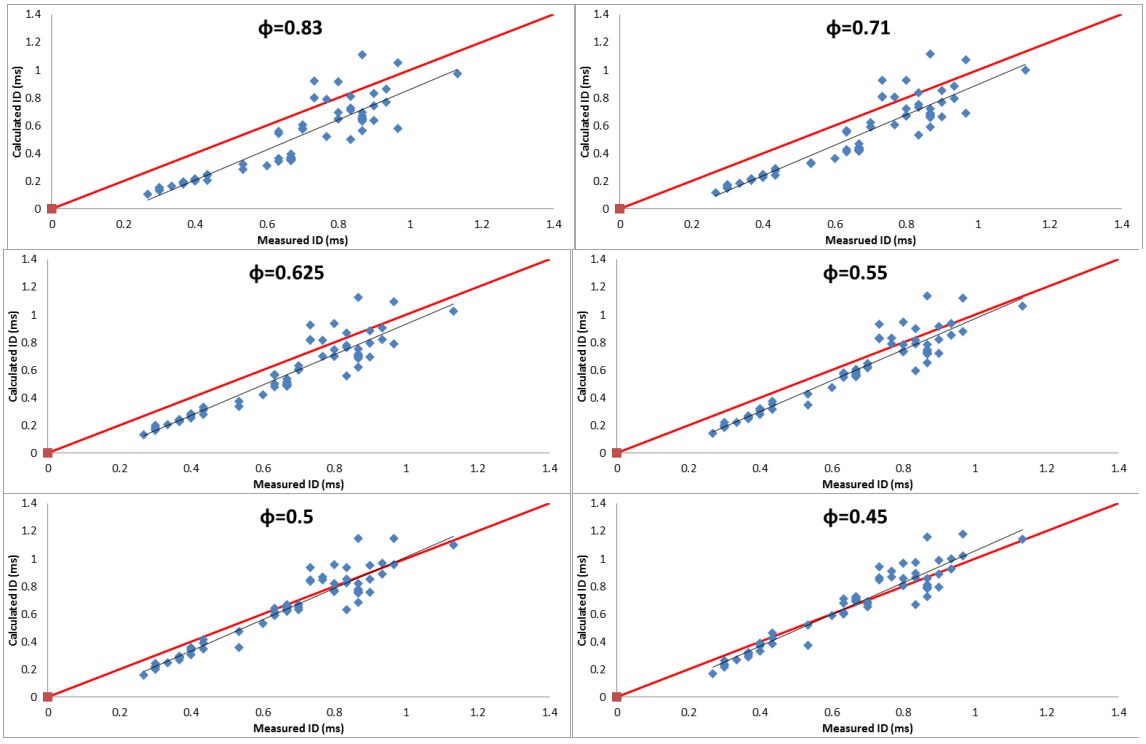

Figure 55: Calculated versus measured ignition delays (ID) for all points for different assumed equivalence ratios (φ). The red line denotes a perfect agreement and the blue line the model predictions.

From the plots above it is clear that the best results are obtained with equivalence ratio values between 0.45 and 0.5. These values are close to the global values of equivalence ratio of this engine setup, which range from around 0.55 to 0.4, depending on the load. Nonetheless this match is thought to be only caused by coincidence, since the actual conditions at the eventual ignition time and location

are likely to be much richer. With this in mind, the equivalence ratio in this model can be used as an extra tuning factor, as was the case in this study.

6.4 Conclusions

In this study a 3-Arrhenious expression was used to calculate the ID from a direct injection medium speed diesel engine. This model was developed using shock tube data and was used in place of a simpler single-Arrhenius approximation in order to improve the predictive capabilities at widely varying charge air temperatures. The model has a single tuning factor, which is the equivalence ratio. This is necessary since the models originate from homogeneous shock tube experiments, and in this application they are used for predictions in a heavily stratified direct injection engine. The model showed very good predictive capabilities of ID for values of equivalence ratio between 0.5 and 0.45, with quite low sensitivity on the choice of equivalence ratio around these values.

6.5 Major achievements

- Use of a 3-Arrhenious ID model for predictions in a direct injection medium speed diesel engine
- Determination of appropriate equivalence ratio inputs for this application
- Improvement of the predictive capabilities for ID when compared to single-Arrhenious expressions, especially at broad temperature ranges.

7 Work package AP5

In addition to annual and intermediate reports submitted to the Swiss Federal Office of Energy, final reports for the co-funding projects are documented in [2,12,66,68].

A number of journal publications have been accepted [32,36,37,41,67] or are under review [49].

Various peer reviewed articles and conference proceedings are documented in [4,6,10 ,40,64,65] and, in conjunction with four invited talks [40,69,70,71] and presentations at workshops [52,53], ensure visibility and dissemination of the achieved results.

References

[1] Obrecht, P. (2012): „Rechenprogramm zur Berechnung des Wärmeentwicklungsgesetzes, Teil 1: Grundlagen und verwendete Algorithmen“, *ETHZ-LAV internal documentation*

[2] Bloch P., Schneider B., Kreutner W., Caruso S, Bargende M. und Boulouchos, K. (2011): „Untersuchungen zur optimalen Zusammensetzung synthetischer Kraftstoffe für konventionelle Diesel-Brennverfahren“. Abschlussbericht über das FVV-Vorhaben Nr. **940**

[3] Gerke, U. (2007): Numerical Analysis of Mixture Formation and Combustion in a Hydrogen Direct-Injection Internal Combustion Engine, *Dissertation ETH Zürich, No.* **17477**

[4] Schlatter, S., Schneider, B., Wright, Y.M. & Boulouchos, K.: “Experimental Study of Ignition and Combustion Characteristics of a Diesel Pilot Spray in a Lean Premixed Methane/Air Charge using a Single Stroke Machine”, *SAE Technical Paper No. 2012-01-0825*

[5] Liu, S., Hewson, J.C., Chen, J.H. & Pitsch, H. (2004): “Effect of strain rate on high-pressure nonpremixed n-heptane autoignition in counterflow”, *Combustion and Flame* **137**, 320-339

[6] Schlatter, S., Wright, Y.M., Schneider, B. and Boulouchos, K.: “3D-CRFD Combustion Modeling of Gas Engines with Pilot Injection”, *Proc. 6th Dessau Gas Engine Conference*, Dessau, Germany, 24th/25th March 2011

[7] Weller, H. G., Uslu, S., Gosman, A.D., Maly, R. R., Herweg, R. and Heel, B. (1994): “Prediction of Combustion in Homogeneous-Charge Spark-Ignition Engines”. *3rd Int. Symp. On Diagnostics and Modeling of Combustion in Internal Combustion Engines*, Yokohama, Japan.

[8] Heel, B., Maly, R., Weller, H. G. and Gosman, A.D. (1998): “Validation of SI combustion model over range of speed, load, equivalence ratio and spark timing”. *Proc. 4th Int. Symp. On Diagnostics and Modeling of Combustion in Internal Combustion Engines*, 255-260.

[9] Gülder , Ö.L. (1991): “Turbulent premixed flame propagation models for different combustion regimes”, *Symp. Int. Comb.* **23**, 743-750

[10] Walther, H.Ph., Schlatter, S., Wachtmeister, G. & Boulouchos, K. (2012): “Combustion Models for Lean-Burn Gas Engines with Pilot Injection,” *peer reviewed article in MTZ worldwide* **2/2012**, 56-73

[11] O'Brien, E. E. & Jiang, T.-L. (1991): “The conditional dissipation rate of an initially binary scalar in homogeneous turbulence”, *Phys. Fluids* **3**, 3121-3123

[12] Walther, H.Ph., Schlatter, S., Wright, Y.M., Wachtmeister, G. & Boulouchos, K. (2012): „Erstellung eines phänomenologischen Modells zur Vorausberechnung des Brennverlaufes von Gasmotoren mit Piloteinspritzung“, *Final report FVV Project No. 960 „Piloteinspritzung“*, **Heft R 951**

[13] Roomina, M.R. & Bilger, R.W. (2001): “Conditional Moment Closure (CMC) Predictions of a Turbulent Methane-Air Jet Flame”, *Combustion and Flame* **125**, 1176-1195

[14] Devaud, C.B. Bray, K.N.C. (2003): “Assessment of the applicability of conditional moment closure to a lifted turbulent flame: first order model”, *Combustion and Flame* **132**, 102-114

[15] Kim, I.S. & Mastorakos, E. (2004): “Simulations of turbulent lifted jet flames with two-dimensional conditional moment closure”, *Proc. Combust. Inst.* **30**, 911-918

[16] Fairweather, M. & Woolley, R.M. (2004): “First-order conditional moment closure modeling of turbulent, non-premixed methane flames”, *Combustion and Flame* **138**, 3-19

[17] Kim, I.S. & Mastorakos, E. (2006): “Simulations of Turbulent Non-Premixed Counterflow Flames with First-Order Conditional Moment Closure”, *Flow, Turbulence and Combustion.* **76**, 133-162

[18] Navarro-Martinez, S. & Kronenburg, A. (2007): “LES-CMC simulations of a turbulent bluff-body flame”, *Proc. Combust. Inst.* **31**, 1721-1728

[19] Navarro-Martinez, S. & Kronenburg, A. (2009): “LES–CMC simulations of a lifted methane flame”, *Proc. Combust. Inst.* **32**, 1509-1516

[20] Fairweather, M. & Woolley, R.M. (2007): “Conditional moment closure calculations of a swirl-stabilized, turbulent non-premixed methane flame”, *Combustion and Flame* **151**, 397-411

[21] Triantafyllidis, A., Mastorakos, E. & Eggels, R.L.G.M. (2009): "Large Eddy Simulations of forced ignition of a non-premixed bluff-body methane flame with Conditional Moment Closure", *Combust. Flame* **156**, 2328-2345

[22] Patwardhan, S.S., Santanu De, Lakshmisha, K.N. & Raghunandan, B.N. (2009): "CMC simulations of lifted turbulent jet flame in a vitiated coflow", *Proc. Combust. Inst.* **32**, 1705-1712

[23] Garmory, A. & E. Mastorakos (2010): "Capturing localised extinction in Sandia Flame F with LES-CMC", *Proc. Combust. Inst.* **33**, 1673-1680

[24] Kim, S.H., Huh, K.Y. & Fraser, A.R. (2000): "Modeling Autoignition in Turbulent Methane Jet by the Conditional Moment Closure Method", *Proc. Combust. Inst.* **28**, 185-191

[25] De Paola, G., Kim, I.S. & Mastorakos, E. (2009) : "Second-Order Conditional Moment Closure Simulations of Autoignition of a n-heptane Plume in a Turbulent Coflow of Heated Air", *Flow, Turbulence and Combustion* **82**, 455-475

[26] El Sayed, A., Milford, A. & Devaud, C.B. (2009): "Modelling of autoignition for methane-based fuel blends using Conditional Moment Closure", *Proc. Combust. Inst.* **32**, 1621-1628

[27] Stanković, I., Triantafyllidis, A., Mastorakos, E., Lacor, C. & Merci, B. (2010): "Simulation of Hydrogen Auto-Ignition in a Turbulent Co-flow of Heated Air with LES and CMC Approach", *Flow Turbulence and Combustion* **86**, 689-710.

[28] Ayache, S. & Mastorakos, E. (2012): "Conditional Moment Closure/Large Eddy Simulation of the Delft-III Natural Gas Non-premixed Jet Flame", *Flow Turbulence and Combustion* **88**, 207-231

[29] Kim, W.T. & Huh, K.Y. (2002): "Numerical Simulation of Spray Autoignition by the First-Order Conditional Moment Closure Model", *Proc. Combust. Inst.* **29**, 569-576

[30] Bottone, F. Kronenburg, A., Marquis, A.J., Gosman, A.D. & Mastorakos, E.: "The numerical simulation of Diesel spray combustion with LES-CMC", *Proceedings of the European Combustion Meeting 2011*

[31] (c) cd-adapco Thermofluid analysis software: www.cd-adapco.com

[32] Wright, Y.M., De Paola, G., Mastorakos, E. & Boulouchos, K. (2009): "Multi-dimensional Conditional Moment Closure modelling applied to a heavy-duty common-rail Diesel engine", *SAE Int. J. Engines **2** (I), 714-726*

[33] Huh, K.Y. & Gosman, A.D. (1991): "A phenomenological model of diesel spray atomization", *Proc. Int. Conf. on Multiphase Flows*, Tsukuba, Japan

[34] Reitz, R. D. & Diwakar, R. (1987): "Structure of High-Pressure Fuel Sprays", *SAE technical paper no. **870598***

[35] Klimenko, A. Y. & Bilger, R. W. (1999): "Conditional Moment Closure for turbulent combustion". *Prog. Energy Combust. Sci.* **25**, 595-687

[36] Wright, Y.M., De Paola, G., Boulouchos, K. & Mastorakos, E. (2005): "Simulations of spray auto-ignition and flame establishment with two-dimensional CMC", *Combustion and Flame **143**, 402-419*

[37] De Paola, G., Mastorakos, E., Wright, Y.M. & Boulouchos, K (2008).: "Diesel engine simulations with multi-dimensional Conditional Moment Closure", *Combustion Science and Technology **180**, 883-899*

[38] Bertola, A.G. (2003): "Technologies for Lowest NO_x and Particulate Emissions in DI-Diesel Engine Combustion – Influence of Injection Parameters, EGR and Fuel Composition", *PhD Thesis, ETH Zürich, Switzerland, Diss. ETH No.* **15373**

[39] Directive 1999/96/EC, December 13, 1999

[40] Wright, Y.M., Bolla, M., Boulouchos, K., Borghesi, G. and Mastorakos, E. (2010): "Conditional Moment Closure For Two-Phase Flows – A Review Of Recent Developments And Application To Various Spray Combustion Configurations", *to appear in Proceedings of the 8th International Conference of Computational Methods in Sciences and Engineering*, Kos, Greece, 3rd – 8th October 2010

[41] Wright, Y.M., Margari, O.-N., Boulouchos, K., De Paola, G., & Mastorakos, E. (2010): "Experiments and Simulations of n-Heptane Spray Auto-Ignition in a Closed Combustion Chamber at Diesel Engine Conditions", *Flow, Turbulence and Combustion **84**, 49-78*

[42] Bikas, G. (2001): "Kinetic Mechanisms for Hydrocarbon ignition", *PhD Thesis, University of Aachen*, Germany

[43] Celik, I., Yavuz, I. & Smirnov, A. (2001): “Large eddy simulations of in-cylinder turbulence for internal combustion engines: a review”, *Int. J. Engine Research* **2** (2), 199-148

[44] Liu, K. & Haworth, D.C. (2010): “Large-eddy simulation for an axisymmetric piston-cylinder assembly with and without swirl”, *Flow, Turbulence and Combustion* **85**, 279–307

[45] Navarro-Martinez, S., Kronenburg, A. & Di Mare, F. (2005): “Conditional moment closure for large eddy simulations”, *Flow, Turbulence and Combustion* **75**, 245–274

[46] Triantafyllidis, A. & Mastorakos, E. (2010): “Implementation issues of the conditional moment closure model in large eddy simulations”, *Flow, Turbulence and Combustion* **84**, 481-512

[47] Koss, H. J., Brüggemann, D., Wiartalla, A., Bäcker, H., Breuer, A. (1992): “Investigations of the Influence of Turbulence and Type of Fuel on the Evaporation and Mixture Formation in Fuel Sprays”, *Final Report of JOULE Project on Integrated Diesel European Action* (IDEA)

[48] Pickett, L. M., (2011): “Engine Combustion Network,”
http://www.sandia.gov/ecn/dieselSprayCombustion.php

[49] Bolla, M., Wright, Y.M. & Boulouchos, K. (2011): “Soot formation modeling of n-Heptane sprays under Diesel engine conditions using the Conditional Moment Closure approach,” *under review for Combustion Sci. and Tech*.

[50] Leung, K. M., et al. (1991), "A Simplified Reaction-Mechanism for Soot Formation in Nonpremixed Flames," *Combustion and Flame* **87**, 289-305

[51] Idicheria, C. A. and Pickett, L. M., (2006) “Formaldehyde Visualization Near Lift-off Location in a Diesel Jet,” *SAE Technical Paper* **2006-01-3434**

[52] Bolla, M., Wright, Y.M. & Boulouchos, K. (2011); ”Soot formation modeling of n-Heptane sprays under Diesel engine conditions using the Conditional Moment Closure approach,” *presented at FIRST Soot Workshop*, DLR Stuttgart, Germany, 26-27 September 2011

[53] Bolla, M., Wright, Y.M. & Boulouchos, K. (2011): ”Soot formation modeling of n-Heptane sprays under Diesel engine conditions using the Conditional Moment Closure approach,” *presented at Tagung der Verbrennungsforschung in der Schweiz*, ETH Zurich, Switzerland, 28 October 2011

[54] Herrmann, K., Schulz, R. and Weisser, G. (2007): “Development of a reference experiment for large diesel engine combustion system optimization”, *CIMAC paper no.* **98**, Vienna, Austria

[55] Herrmann, K., Kyrtatos, A., Schulz, R., Weisser, G.A. von Rotz, B., Schneider, B. and Boulouchos, K. (2009): *Proceedings of the 11th Triennial International Annual Conference on Liquid Atomization and Spray Systems*, Vail, Colorado USA.

[56] Bolla, M., Cattin, M., Wright, Y.M., Boulouchos, K. & Schulz, R.: “3D-CFD Lagrangian Spray Simulations for Large two Stroke Marine Diesel Engines Compared with Experimental Data of a Spray Combustion Chamber”, *to be presented at the ASME 2012 Internal Combustion Engine Spring Technical Conference,* ***ICES2012-81016***, Torino, Italy, 6th – 9th May 2012

[57] Pizza, G., Wright, Y.M., Weisser, G. & Boulouchos, K.: “Evaporating and non-evaporating Diesel spray simulation: Comparison between the ETAB and WAVE breakup model”, *Int. Journal of Vehicle Design* ***45****, 80-99*.

[58] Schulz, R., Herrmann, K., von Rotz, B., Hensel, S., Seling, F., Weisser, G., Wright, Y.M., Bolla, M. & Boulouchos, K. (2010): “Assessing the Performance of Spray and Combustion Simulation Tools against Reference Data Obtained in a Spray Combustion Chamber Repre-sentative of Large Two-Stroke Diesel Engine Combustion Systems, *CIMAC paper no.* **247**, Bergen, Norway

[59] von Rotz, B., Herrmann, K., Weisser, G., Cattin, M., Bolla, M. and Boulouchos, K. (2011): ”Impact of Evaporation, Swirl and Fuel Quality on the Characteristics of Large 2-Stroke Marine Diesel Engine Combustion Systems,” *Proceedings of ILASS-Europe*, Estoril, Portugal, September 2011

[60] Schmid, A., von Rotz, B., Bombach, R., Weisser, G., Herrmann, K. & Boulouchos, K. (2012): “”, *accepted for publication in COMODIA,* Fukuoka, Japan, 21st – 26th July 2012

[61] Bolla, M., Wright, Y.M. & Boulouchos, K. (2012): “Application of a Conditional Moment Closure Combustion model to a large two-stroke marine Diesel engine reference experiment*”, accepted for publication in COMODIA,* Fukuoka, Japan, 21st – 26th July 2012

[62] Peters, N. (2000): “Turbulent combustion”, *Cambridge University Press*

[63] Venugopal, R. and Abraham, J. (2007): “A Review of Fundamental Studies Relevant to Flame Lift-off in Diesel Jets”, *SAE Technical paper no.* **2007-01-0134**

[64] Kyrtatos, P., Obrecht, P., Boulouchos, K., Hoyer, K., Gatel, G. and Dietrich, P. (2009): Combustion and emission analysis in a 4-stroke common rail medium-speed large Diesel engine, *12. Tagung "Der Arbeitsprozess des Verbrennungsmotors"*, Graz, Austria

[65] Kyrtatos, P., Obrecht, P., Hoyer, K., Boulouchos, K. (2010): Predictive Simulation and Experimental Validation of Phenomenological Combustion and Emission Models for Medium-Speed Common Rail Engines at Varying Inlet Conditions, *CIMAC Congress 2010 Paper No.* **143**, Bergen, Norway

[66] Vandersickel, A., Mitakos, D., Schneider, B. & Boulouchos, K. (2011):,“Brennstoffe für homogene selbstgezündete Verbrennungsprozesse”, *Final Report to the Swiss Federal Office of Energy (BfE), project* **101,514**

[67] Vandersickel, A., Hartmann, M., Vogels, K., Wright, Y.M., Fikri, M., Starke, R., Schulz, C. & Boulouchos, K. “The autoignition of practical fuels at HCCI conditions: High-pressure shock tube experiments and phenomenological modeling”, *FUEL* **93**, 492-501

[68] Wright Y.M, Bolla M., Wilhelm P., Jahnson P., Kyrtatos P., Obrecht P., Kirchen P., Barro C., (2010): “Clean and Efficient Large Diesel Engines (CELaDE)”, *Final report to the Competence Centre Energy and Mobility (CCEM)*

[69] Wright, Y.M. (2011): “Large marine engine modelling - From 0.5 litres to 0.5 m3 displacement – three orders of magnitude of spray combustion with Conditional Moment Closure”, *Invited talk held at the spring technical meeting of the Institute of Physics, Combustion physics group*, Southampton, UK, 23rd May 2011

[70] Wright, Y.M. (2009): ”State-of the art combustion modelling with Conditional Moment Closure”, *Invited talk held at the cd-adapco European Internal Combustion Engine workshop*, London, UK, 24. März 2009

[71] Wright, Y.M. (2009): ”State-of the art combustion modelling with Conditional Moment Closure”, *Invited talk held at the cd-adapco North American Internal Combustion Engine workshop*, Novi Detroit, MI, USA, 25. April 2009

Appendix

Blend Name	Ref fuel CEC RF06-03	FT1 180-310	FT1 + 20%v naphtens	FT1 + 20%v iso-paraffins	FT1 + 20%v oléfins	FT2 130-310	FT1 + 20%v mono-aromatics	FT1+ 20% heavy alcohols
Abbreviation	RDF	FT-Base	FT-Naph	FT-iPar	FT-Olef	FT-IIBP	FT-Arom	FT-Alc
Ref Nr	*8000*	*7780*	*7749*	*7750*	*7755*	*7765*	*7766*	*7774*
Cetane number (-)	53	72.2*	62.7	63.5	66.7	62.4	57.9	62.1
Density (15°C) (kg/m3)	834.4	788.1	804.6	789.7	786.7	772.1	807	797.7
Sulfur content (mg/kg)	6	17	31	19	22	22	21	20
Flash point (°C)	65	89	92	87	93	39	73	89
HFRR (lubricity) 60°C (µm)	370	334	377	309	342	331	337	424
Kin. viscosity (40°C) (mm2/s)	2.711	2.354	2.501	2.244	2.261	1.654	1.758	2.817
Calorific value, lower (J/g)	42900	44061	43730	44093	43841	43853	42905	42778
Carbon content (%(m/m))	86.4	85.2	85.35	84.85	85.23	84.86	86.11	83.29
Hydrogen content (%(m/m))	13.5	15	14.83	15.24	14.91	15.2	13.99	14.9
Oxygen content (%(m/m))	< 0.5	< 0.5	< 0.5	< 0.5	< 0.5	< 0.5	< 0.5	1.80
Nitrogen content (mg/kg)		< 0.5	< 1	< 1	< 1	< 1	< 1	< 1
H/C	1.862	2.098	2.071	2.140	2.085	2.134	1.936	2.132
O/C								0.016
A/F-Ratio	14.540	14.915	14.874	14.957	14.888	14.944	14.674	14.584
Distillation								
IBP (°C)	163	188.4	189.3	173	194.4	134	185.6	193.2
5% (V/V) rec. at (°C)	187	211.1	215.2	192.3	215.4	140	187	213
10% (V/V) rec. at (°C)	198	215.5	222.8	196.9	219.4	159.2	189.4	217
20% (V/V) rec. at (°C)	219	225.7	232.2	200.8	230	182	196.8	228.4
30% (V/V) rec. at (°C)	240	236.4	243.8	231.9	239.4	203.8	209	238.8
40% (V/V) rec. at (°C)	263	247.5	253.8	238.5	248.6	221.8	222.4	248.2
50% (V/V) rec. at (°C)	279	257.3	262.2	251.6	258	236.2	236.4	256.8
60% (V/V) rec. at (°C)	298	265.8	270.8	264.8	267.6	250.4	251	264.4
70% (V/V) rec. at (°C)	311	273.7	279.4	279.7	277.2	264.4	265	271.8
80% (V/V) rec. at (°C)	322	281.9	287.4	295	286.2	277	277.6	280.2
90% (V/V) rec. at (°C)	334	291.3	297	310	294.4	289.2	289.4	291.2
95% (V/V) rec. at (°C)	346	297.6	303.8	318.5	298.4	297.6	297.6	298.8
FBP (°C)	355	303	314	337.1	305.6	306.6	306.6	306.7
% (V/V) rec. at 250°C	34.2	42.5	35.7	53.1	41.6	59.7	59.4	42.1
% (V/V) rec. at 350°C	96	> 98	> 98	> 99	> 98	> 98	>98	n.B.

*) CZ Measurement by SGS Speyer

Table 7: Composition of the fuels investigated in Work Package 2a.

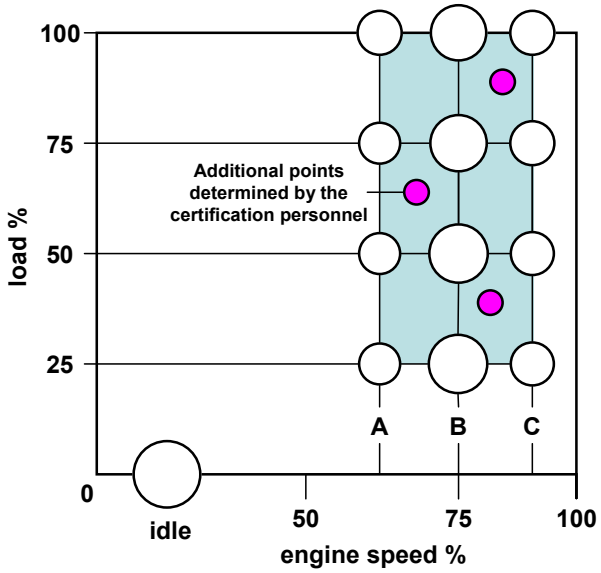

Figure 56: European steady cycle test map, source: http://www.dieselnet.com

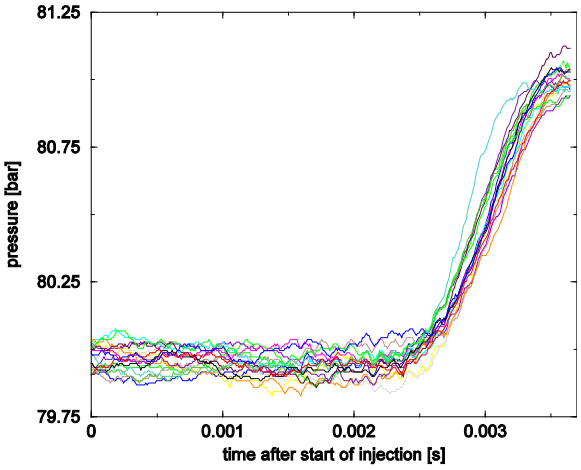

Figure 57: Recorded pressure traces for 17 individual realisations; sample rate is 200 kHz. The raw data has been smoothed by 50-point running averages. Total injection duration 1.65 ms (physical). Source [41].

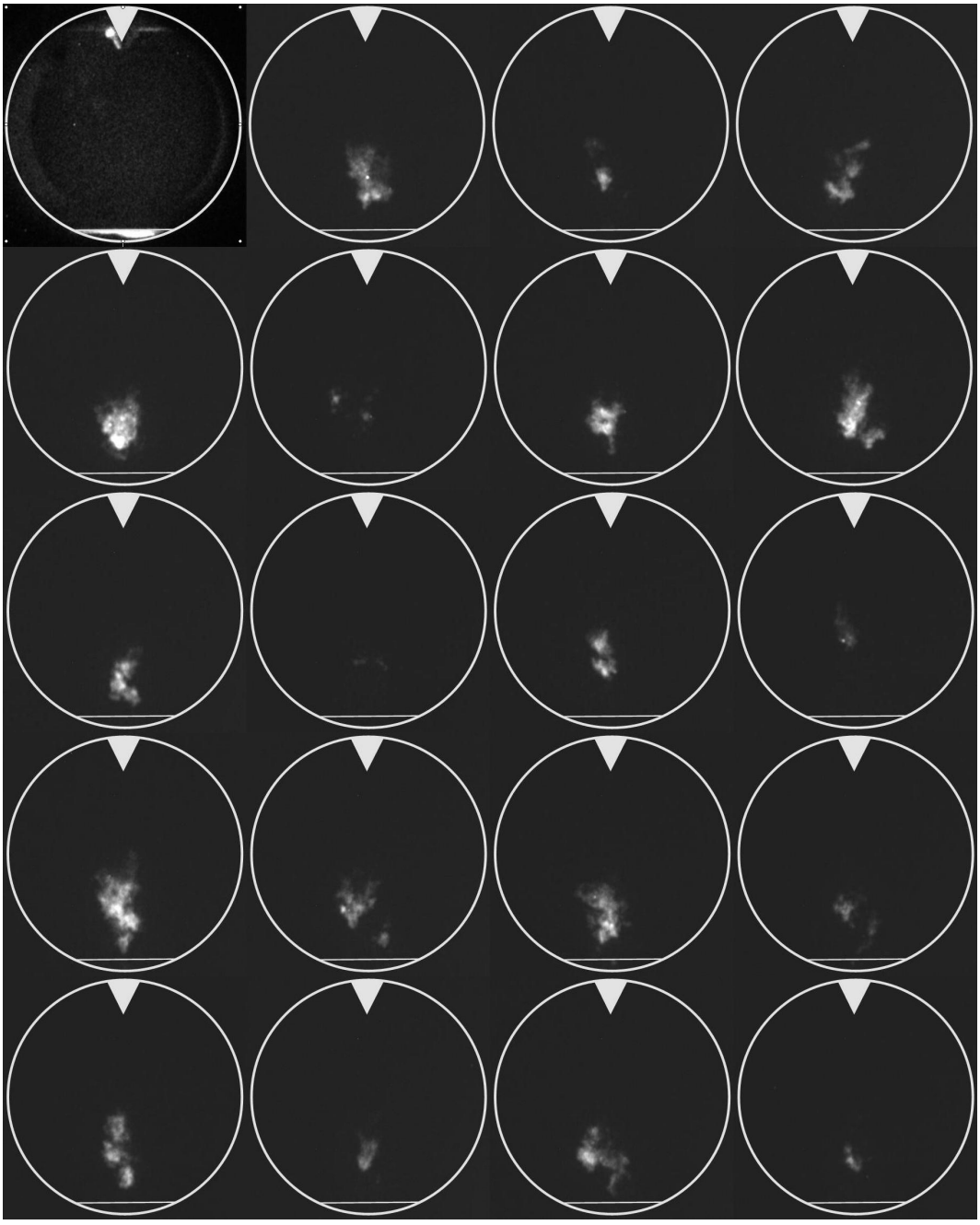

Figure 58: Selection of 19 chemiluminescence images at the time of ignition (2.5 ms after start of injection) showing the substantial variation of the ignition location. The top left image has been used for background subtraction and to determine window, injector and wall locations shown by the ring, triangle and line, respectively. Source [41].

Acronyms

2D / 3D	Two- / three-dimensional
AMC	Amplitude Mapping Closure
BDC (a/b)	Bottom Dead Centre (after/before)
BfE / SFOE	Bundes-Amt für Energie / Swiss Federal Office of Energy (Swiss funding agency)
BMEP	Brake Mean Effective Pressure
CA	Crank angle
CCEM	Swiss Competence Centre for Energy and Mobility (Swiss funding agency)
CMC	Conditional Moment Closure
CN/CZ	Cetane Number / Cetan-Zahl
CR	Common-Rail
CRFD	Computation Reactive Fluid Dynamics
DI	Direct Injection
ECU	Engine Control Unit
EGR	Exhaust Gas Recirculation
EOI	End Of Injection
ETH	Eidgenössische Technische Hochschule (Swiss Federal Institute of Technology)
FT	Fischer-Tropsch
FVV	Forschungs-Vereinigung Verbrennungskraftmaschinen (German funding agency)
HFO	Heavy Fuel Oil
HRR	Heat Release Rate
HTDZ	High temperature, high pressure test rig of LAV, ETH Zurich
ID	Ignition Delay
IVC	Intake Valve Closure
KTI	Swiss Innovation Promotion Agency
LAV	Aerothermochemistry and combustion systems Laboratory of ETH Zurich
LES	Large Eddy Simulation
NO_x	Nitric oxides (NO and NO_2)
RANS	Reynolds Averaged Navier Stokes
RDF	Reference Diesel Fuel
RPM	Revolution Per Minute (engine speed)
SAE	Society of Automotive Engineers
SOI (a)	Start of Injection (after)
TDC (a/b)	Top Dead Centre (after/before)
WEG	Wärme-Entwicklungs-Gesetz (pressure data analysis/post-processing tool)

Table 8: Acronyms.